Title

Numerical investigation of air intrusion and aerobic reactions in municipal solid waste landfills

Authors

Fathinezhad, Alborz
Jafari, Navid H
Oldenburg, Curtis M
et al.

Publication Date

2022-06-01

DOI

10.1016/j.wasman.2022.05.009

NUMERICAL INVESTIGATION OF AIR INTRUSION AND AEROBIC REACTIONS IN MUNICIPAL SOLID WASTE LANDFILLS

Alborz Fathinezhad
Dept. of Civil and Environmental Engineering
Louisiana State University
Baton Rouge, LA 70803
Email: falbor1@lsu.edu

Navid H. Jafari, Ph.D., A.M. ASCE
Assistant Professor of Civil and Environmental Engineering
Louisiana State University
Baton Rouge, LA 70803
Email: njafari@lsu.edu

Curtis M. Oldenburg, Ph.D.
Senior Scientist
Energy Geosciences Division
Lawrence Berkeley National Laboratory
Email: cmoldenburg@lbl.gov

Michael D. Caldwell
Director, Groundwater and Technical Program
Waste Management, Inc.
Houston, TX
Email: mcaldwell@wm.com

Open Access version of the following published paper to which citations should be made:

Fathinezhad, A., Jafari, N.H., Oldenburg, C.M. and Caldwell, M.D., 2022. Numerical investigation of air intrusion and aerobic reactions in municipal solid waste landfills. *Waste Management*, *147*, pp.60-72.
https://doi.org/10.1016/j.wasman.2022.05.009

October 3, 2022

Numerical Investigation of Air Intrusion and Aerobic Reactions in Municipal Solid Waste Landfills

Alborz Fathinezhad[1,*], Navid H. Jafari[2], Curtis M. Oldenburg[3], and Michael D. Caldwell[4]

[1] Graduate Research Assistant, Dept. of Civil and Environmental Engineering, Louisiana State University, 3252 Patrick Taylor Hall, Baton Rouge, LA 70803. E-mail: falbor1@lsu.edu
[2] Assistant Professor, Dept. of Civil and Environmental Engineering, Louisiana State University, 3504 Patrick Taylor Hall, Baton Rouge, LA 70803. E-mail: njafari@lsu.edu
[3] Senior Scientist, Energy Geosciences Division, Lawrence Berkeley National Laboratory, Berkeley, CA. E-mail: cmoldenburg@lbl.gov
[4] Director, Groundwater Protection and Technical Programs, Waste Management Inc., Houston, TX. E-mail: mcaldwell@wm.com
[*] Corresponding author.

ABSTRACT: Air intrusion into municipal solid waste landfills can cause a localized switch from anaerobic to aerobic biodegradation adjacent to the intrusion. The purpose of this study was to explore the effects on temperature and gas composition of air intrusion into an idealized anaerobic landfill. Two scenarios of air intrusion and injection were simulated using a mechanistic landfill model built into TOUGH2. The modeled landfill geometry and properties are based on an actual U.S. landfill. The simulation results show that air intrusion can cause a quick switch from anaerobic to aerobic conditions and as a result, cause a fast increase in temperature of up to 30ºC associated with stimulation of aerobic biodegradation reactions. Associated with the change to aerobic conditions is a decrease in CH_4/CO_2 (v/v) ratio in the landfill gas. Depending on the air flow rate intruding or injecting into the landfill, localized aerobic biodegradation is stimulated and as a result heat flux of 10 to 150 W/m^3 leads to temperature increase. Temperature increase near the interim system lasts no longer than few weeks while the high temperatures in deep layers could last up to one year.

Keywords: aerobic biodegradation, modeling municipal solid waste, biodegradation of municipal solid waste, landfill gas generation

1. INTRODUCTION

Municipal solid waste (MSW) landfills are designed and constructed to operate under a temperature regime that allows anaerobic biological processes to decompose organics into methane gas as a renewable energy resource (National Research Council 2007). However, there is an increased awareness in the solid waste industry that industrial and special wastes co-disposed in MSW landfills can result in chemical reactions that generate and accumulate heat within the waste, thus raising temperatures above the threshold of anaerobic biological processes (assumed as exceeding 65°C or 150°F; Hartz et al. 1982; Kasali et al. 1989; Yeşiller et al. 2005; Zinder 1993). Examples of exothermic industrial wastes include aluminum production wastes, MSW incinerator ash, coal bottom ash, lime/cement kiln dust, and fly ash (Jafari et al. 2017; Klein et al. 2001, 2003). The associated chemical reactions involve the corrosion of aluminum and iron (Calder and Stark 2010; Jafari et al. 2014), along with hydration and carbonation of calcium oxide and calcium hydroxide (Narode et al. 2021), respectively. Another possible contributor to heat generation and accumulation is the introduction of air into a landfill during gas collection and control operations. This is separate from landfill aeration (Ritzkowski and Stegmann 2012), which explicitly uses forced air injection to promote the aerobic biodegradation of MSW to mitigate CH_4 emissions and enhance the rate of waste stabilization (Read et al. 2001). For example, Haug (2018) observed temperatures of 70°C when air was injected into enclosed cells composed of wastewater treatment sludge over 24 days. Themelis and Kim (2002) monitored a 600 m^2 by 3 m deep aerobic cell and reported that 75% of heat generated from aerobic reactions was retained in the waste, with 25% heat loss occurring due to natural convection and radiation to the surroundings. These demonstration studies imply that while air injection can accelerate waste stabilization, it also creates a significant challenge by accumulating heat (Merz and Stone 1962). As a result, there is a need to quantify the magnitude and rate of heat generation based on air flux, spatial extent of aerobic reactions, and rate of heat dissipation. Hashemi et al. (2002) and Sanchez et al. (2006) developed a 3D model of gas generation and transport in a hypothetical landfill and investigated the effects of various physical properties of porous on gas pressure, fluid transfer, temperature. Hao et al. (2020) modeled 3D hypothetical landfill to estimate heat generation, transport, and accumulation. Their result showed that ash disposal causes temperature increase to 200°C within first 6 years of landfilling.

In this study, possible pathways of air intrusion into landfills were simulated to understand their potential contribution to heat generation and accumulation, along with moisture redistribution, in the waste mass. The TOUGH2 Landfill Bioreactor Model (T2LBM; Oldenburg 2011) was used to simulate multiphase flow in an idealized landfill undergoing either anaerobic or aerobic biodegradation depending on the local oxygen concentration. An idealized 2-D landfill model was developed based on an operating landfill in the Midwest, with three MSW layers representing waste of varying ages with a static initial moisture distribution as controlled by gravity and capillary pressure, and undergoing anaerobic biodegradation with active gas extraction wells. Air intrusion was modeled as occurring due to gas extraction wells unintentionally pulling air into the waste mass through cracks in the soil cover, and secondly as leaks in air lines used to pressurize gas well liquid pumps that remove condensate and leachate collected inside gas extraction well pipes. As air permeates into the landfill from these hypothetical sources, the spatial and temporal changes in temperature, gas composition, pressure, and flow rate, and liquid saturation are simulated and mapped to discern the zone of influence of aerobic reactions and the duration of higher temperatures and oxygen that remain in the landfill after the air intrusion has been remediated. As previously stated, the air line leak included in this study was based loosely on an actual air line leak event at an MSW landfill in the southern US. The input parameters (such as line diameter, flow rate, and generalized depth) were obtained from field personnel associated with the landfill operation.

While the potential for subsurface oxidation events from overpulling of air into the waste mass from gas extraction wells is well understood in the solid waste industry, the magnitude and reaction times from a larger scale air intrusion, such as an air line break, has not been modeled. Such a numerical investigation of air intrusion and aerobic reactions can also serve to inform the magnitude of temperature propagation from a larger scale event. The results of this study can enable practitioners and regulators to quantify the complex and coupled biological, thermal, and flow behaviors of landfills under changing anaerobic-aerobic conditions. It could also facilitate a better understanding of the short- and long-term implications to of air intrusion to landfill operations and maintenance, including reduced renewable energy production, localized differential settlement, and reduced service life of geosynthetics (Jafari et al. 2014).

2. T2LBM BIODEGRADATION REACTIONS

The TOUGH2 Landfill Bioreactor Model (T2LBM) (Oldenburg 2001) was built onto TOUGH2 to allow mechanistic simulation of a simplified set of aerobic and anaerobic landfill biodegradation reactions, along with the non-isothermal multiphase and multicomponent flow and transport simulated by TOUGH2 (Pruess et al. 1999). T2LBM incorporates the biodegradation of a single mobile biodegradable substrate proxy (MBSP) that represents all of the biodegradable material in the MSW. This approach assumes implicitly that early stages of anaerobic or aerobic biodegradation of organics previously occurred (hydrolysis, acetogenesis, and acidogenesis) and places the model focus on the last biodegradation step of methanogenesis (landfill gas production) through biodegradation of the MBSP. The earlier phases of biodegradation involving the formation of MBSP can be phenomenologically modeled by the user through inputs that specify various local initial concentrations or variable generation rates of MBSP (Oldenburg 2001). T2LBM uses a Monod kinetic rate law to simulate the biodegradation reactions in the aqueous (liquid) phase of the two-phase (gas and liquid) model system.

T2LBM has been verified by comparison to bench-scale laboratory and field-scale configurations of anaerobic and aerobic treatment of MSW by leachate recirculation, air injection, temperature control, and waste placement as described in Oldenburg (2001). Specifically, the dynamics of aerobic biodegradation simulation of T2LBM were compared and verified with the results from laboratory experiments of Kaiser and Soyez (1990) as documented in Kaiser (1996). The methane production activity during anaerobic biodegradation of a small mass of waste mixed with acetate given by Lay et al. (1998) was simulated and compared with the experimental results. While some properties of the experimental system by Kaiser (1996) was used directly, some other properties were derived due to the specific process model conceptualization of T2LBM. With constraints on many properties of the system prescribed by the experimental specifications, there are at least two important parameters to adjust to fit T2LBM results with the results shown in Kasier (1996). These included the initial mass fraction of MBSP in the liquid, and the single microbial growth rate for the breakdown of a single chemical species (MBSP) as proxy for numerous microbial populations and substrates. Agreement of temperature, CO_2, O_2 consumption between experiment and T2LBM was good.

T2LBM includes five volatile chemical components distributed between gas and liquid phases, which are water (H_2O), nitrogen (N_2), oxygen (O_2), carbon dioxide (CO_2), and methane (CH_4). The biodegradable component, MBSP, resides only in the liquid phase. The solid phase in

T2LBM comprises the grains of the porous medium and is assigned the thermo-physical properties of MSW material. The five volatile components are distributed between the aqueous (liquid) and gas phases as controlled by the local solubility specified by Henry's law.

The substrate utilization rate in T2LBM follows the Monod kinetic rate equation. In general, the rate of substrate utilization in T2LBM is estimated by Eq. (1):

$$\frac{dS}{dt} = -\frac{1}{Y}\left(\frac{dB}{dt} + \delta B\right) = -\frac{1}{Y}\left(\mu_B B + \delta B\right) \tag{1}$$

Eq. (1) describes the mathematical relationship between microbial biomass and nutrient consumption (substrate utilization) in an aqueous environment over time, where S is substrate (MBSP) concentration, Y is yield coefficient, B is bacterial concentration (aerobic or anaerobic depending on the presence or absence of O_2), δ is the microbial death rate, and μ_B is the microbial growth rate. Yield coefficient is the ratio of the amount of biomass produced to the amount of substrate consumed. The microbial growth rate is a function of several parameters in Eq. (2):

$$\mu_B = \mu_{\max,B} f_B^T \frac{S}{K_{S,B} + S} - \delta \tag{2}$$

where $\mu_{\max}$ is the maximum specific growth rate, f_B^T is the coefficient of temperature-dependent growth, and $K_{S,B}$ is the microbial saturation constant. In Eq. (2), μ_{max} and $K_{S,B}$ are empirical coefficients that differ between microorganism species and depend on the ambient environmental conditions, *e.g.*, temperature, pH of the aqueous phase, and composition of the microbial medium.

Temperature dependence of the biodegradation is included through the function f_B^T in Eq. (3):

$$f_B^{\ T} = \frac{T(T_{\max,B} - T)}{\left(\frac{T_{\max,B}}{2}\right)^2} \quad (3)$$

where $T_{max,B}$ is the maximum tolerable temperature for anaerobic and aerobic bacteria, and T is the temperature at any time (°C). In this model, the maximum tolerable temperatures for anaerobic and aerobic biodegradation are assumed to be 65°C and 80°C, respectively (De la Cruz et al. 2021; Jafari et al. 2017; Rowe & Islam 2009; Yazdani et al. 2010; Yeşiller et al. 2005; Zinder 1993) which means at temperatures above these values the biodegradation reaction is inhibited ($f_B^{\ T} = 0$). The idealized aerobic and anaerobic biodegradation reactions modeled in T2LBM follow the formulas in Eqs. (4) – (5), where BA and BN represent Aerobic Biomass and Anaerobic Biomass, respectively. Complete details of the biological reactions in T2LBM can be found in Oldenburg (2001).

$$\text{MBSP} + 2\text{O}_2 \xrightarrow{\textit{Aerobic Bacteria}} 2\text{CO}_2 + 2\text{H}_2\text{O} + \text{Heat} + \text{BA} \quad (4)$$

$$\text{MBSP} \xrightarrow{\textit{Anaerobic Bacteria}} \text{CH}_4 + \text{CO}_2 + \text{Heat} + \text{BN} \quad (5)$$

In this study, T2LBM was used to simulate the spatial and temporal variation in gas, moisture, and heat transfer due to air intrusion, the process by which the MSW landfill biodegradation switches from an anaerobic to aerobic process. Before simulating the air intrusion into the landfill model system described in the next section, an anaerobic simulation was conducted to reach initial conditions found during the methanogenesis stage of MSW, specifically the temperature, fluid pressure, gas composition, and liquid saturation. The transition from anaerobic to aerobic condition in T2LBM is calculated and handled at each iteration, with the results weighted by an arctan switching function:

$$a = \frac{1}{2} + \frac{1}{\pi}\tan^{-1}\left(switchf\,(X_{liq}^{O_2} - X_{critical}^{O_2}) \right) \tag{6}$$

In Eq. (6), a varies from ~1 for $X_{liq}^{O_2} \geq X_{critical}^{O_2}$, to ~0 for $X_{liq}^{O_2} \leq X_{critical}^{O_2}$. The steepness of the transition around $X_{critical}^{O_2}$ is controlled by the user through the variable *switch* in the input file. This approach provides a smooth transition from anaerobic to aerobic conditions. The term aerobicity is given to the function a and is given as primary output from T2LBM to delineate aerobic and anaerobic regions of the domain. This also makes possible that anaerobic reactions be only partially inhibited by air injection, and subsequent aerobic reaction and temperature increase.

3. LANDFILL MODEL SYSTEM

3.1. Landfill Geometry

The idealized 2-D model system in Fig. 1 is representative of a specific Midwest landfill. The 2-D landfill was developed with the bottom and top lengths equal to 356 m and 148 m, respectively, along with a height of 48 m and side slopes of 3H:1V. The landfill domain was discretized into grid blocks of sizes 1 m in the vertical direction and 2 m in the horizontal direction. The model includes five horizontal layers starting from the landfill base as follows: (1) Bottom layer (1 m thick) that serves as a no-flow boundary condition for gas and leachate; (2) Three MSW layers (shallow, intermediate, and deep) that vary in physical, thermal, hydraulic, and biological properties (i.e., density, porosity, specific heat conductivity); and (3) Surface cover layer that was either modeled as a geomembrane or clay cover material with a thickness of 1 m depending on the scenario analyzed. The model system represents initially a closed landfill that is capped with a cover system and is operating under anaerobic conditions for several years until it is subject to air intrusion. In Fig. 1, the thicknesses of shallow and intermediate MSW layers were set to 18 m each, and the deep layer thickness was set to 12 m. The gas extraction wells were located 50 m apart with different slot lengths and extraction rates (see Table S2).

3.2. Boundary Conditions

Conditions of constant atmospheric pressure and temperature (101 kPa and 25ºC, respectively) are maintained at the top of the landfill cover. Various properties of the surface clay cover material are specified to model the sealing properties (no air intrusion) and the failures of the cover (e.g., cracks or other openings) depending on the scenario being simulated. The boundary condition between the deep MSW layer and native foundation (bottom of domain) is modeled to prevent fluid (gas and leachate) advection but allow heat transfer. In TOUGH2, by assigning infinite heat capacity or infinite volume of grid block, the user can create a first-type boundary condition. In this model, infinite specific heat capacity was assigned to the grid blocks of atmospheric grid blocks layer so that the temperature is set and remains at 25°C ($\partial T/\partial t \sim 0$). Very low permeability was assigned to clay layer to prevent any fluid flow transfer. The bottom domain boundary condition is extended to the vertical side walls. Thus, the underlying geology outside of the landfill boundary serves only as a heat sink.

3.3. Material Properties

The thermal-hydraulic-physical material properties for the three MSW layers, along with the clay used as the surface and bottom layers, are summarized in Table 1. The properties were selected to reflect the fact that generally the degree of MSW biodegradation and consolidation increase from shallow to deep layers, e.g., density increases with depth, and porosity and hydraulic conductivity decrease with depth.

The porosity (n) of MSW also decreases with depth to reflect less void space and thus a more compacted waste mass. The case study landfill on which this model is based was filled rapidly over a period of around 8 years. It was assumed that the shallow layer was less than 2 years old. Therefore, the shallow layer is considered to be freshly land-filled MSW, which has undergone limited biological degradation and compaction compared to the older and higher density intermediate and deep layers.

The bulk density of MSW varies from 300 to 1,734 kg/m^3 (equivalent to a unit weight of 3 to 17 kN/m^3), depending on the MSW age and applied stress as measured in laboratory experiments (Beaven 2000; Kavazanjian et al. 1995; Zekkos et al. 2006). The intrinsic permeability of MSW was found based on correlations with MSW density (Staub et al. 2009; Xu et al. 2020). The specific intrinsic permeability values assigned to MSW layers were developed based on the applied stresses estimated in the case study, and the values are within the range reported in Breitmeyer and Benson (2019) and Beaven (2000). To estimate intrinsic permeability, the effective stress in the middle of each MSW layer was related to permeability as a function of normal stress. The estimated effective stress of 60 kPa, 213 kPa, and 360 kPa for the shallow, intermediate, and deep MSW layer, respectively. The results in the study of Beaven (2000) shows that in the same range of applied stress on various MSW samples, the hydraulic conductivity is between 10^{-7} to 10^{-4} m/s, which is equivalent to permeability of 10^{-14} to 10^{-11} m^2 (assuming the density and viscosity of water at ambient conditions).

T2LBM uses intrinsic permeability (k) of a porous medium rather than hydraulic conductivity (K). At 20ºC, the density and dynamic viscosity of water are ρ_w = 1,000 kg/m^3 and η = 1 × 10^{-3} kg/(m·s), respectively. Therefore, one unit of K (m/s) will be approximately equal to 1 × 10^7 units of k (m^2).

$$K = \frac{\rho_w \, g \, k}{\eta_w} \tag{7}$$

The shallow layer density (ρ = 750 kg/m^3) is adapted from Staub (2009), who found the saturated vertical hydraulic conductivity to be K_v =3 × 10^{-5} m/s at an initial volumetric moisture content (θ) of 21% (gravimetric moisture content (w) of 37%) and porosity n = 0.6. This also aligns with Beaven (2000), who reported K_v = 2 × 10^{-5} m/s for an unprocessed-fresh household waste material under applied stresses ranging from σ_v = 0 to 84 kPa and ρ = 700 to 840 kg/m^3. Beaven (2000) indicated that the K_v of an excavated and aged MSW (approximately 20 years old) was 6 × 10^{-6} and 5 × 10^{-7} m/s (k_v = ~5 × 10^{-13} m^2) under applied stresses of 165 and 322 kPa, respectively. Because the K_v of MSW is inversely related to ρ, n, and σ_v (Townsend et al. 2015), it decreases with increasing depth in the landfill. Because field observations of landfills indicate better drainage in the horizontal direction, the MSW is assumed to be anisotropic with k_h that is one order of magnitude higher than k_v (Jain et al. 2006). The soil water retention curves (SWRCs) and hydraulic conductivity functions (HCF) for each MSW layer follow laboratory experiments by Breitmeyer et al. (2019), Breitmeyer and Benson (2014), and Stoltz et al. (2010).

The thermal conductivity (K_T) of MSW ranges from 0.2 to 1.5 W/(m·K) (Faitli et al. 2015; Gholamifard et al. 2008; Rollins et al. 2005). The K_T increases from 0.3 to 0.9 W/(m·K) with depth because higher densities facilitate more particle to particle contact and increasing water content facilitates heat transfer (Yeşiller et al. 2015). The heat capacity (C_p) of MSW typically involves weighted averaging of the heat capacities of the individual of MSW components. For example, Hanson et al. (2008) report the volumetric C_p of MSW landfills located in Michigan, New Mexico, Alaska, and British Columbia as 2, 1.2, 1, and 2.2 MJ/(m^3·K), respectively. The value from the Michigan MSW (C_p = 2 MJ/m^3·K) was used because our study is loosely based on a Midwestern landfill. The volumetric C_p was converted to a specific C_p (J/kg·K) using the density of each MSW layer. A sensitivity analysis was performed on the influence of C_p on heat transfer.

3.4. Gravity Capillary Equilibrium

T2LBM offers a choice of several SWRC functions to simulate the transport of wetting and non-wetting fluid mixtures in unsaturated porous media. Laboratory and field experiments suggest that the van Genuchten (1980) model captures the behavior of MSW (Breitmeyer and Benson 2014; Stoltz et al. 2012). Fig. S1 shows the degree of saturation (S) as a function of matric suction (ψ) for each material layer, and Table S1 lists the TOUGH2 input parameters for van Genuchten (1980) function. To replicate the landfill in Fig. 1 with side slopes, a physically reasonable steady-state simulation is required to reach gravity-capillary equilibrium (static steady-state moisture distribution) before applying the biological reactions. Under partially saturated conditions, gravity will move water down and capillarity can spread water vertically until a steady-state condition is reached (Yortsos 1995). The steady-state condition is subsequently used as the initial conditions for the transient analyses. The generation of gravity-capillary equilibrium for this complex 2-D model is explained in detail in supplemental and shown in Fig. S2.

In the shallow and intermediate MSW layers, the *S* does not vary with depth and remains constant at 32% and 43%, respectively. The matric suction values corresponding to the shallow and intermediate layers are 3.5 kPa, and 1.5 kPa, respectively. In the deep MSW layer, the *S* increases from 50% to 100% at the leachate collection system. The matric suction is less than 1 kPa in this layer. After reaching gravity-capillary equilibrium, the anaerobic biological reactions were initiated. The modeled landfill is assumed to be at a stage where waste acceptance is near completion, a surface cover system is present, and gas extraction wells are operating. At this stage, the model is calibrated such that the MSW layers are undergoing anaerobic biodegradation with the ratio of CH_4 to CO_2 equal to unity and the temperature profiles reflect observed waste temperatures in the methanogenesis stage (Yesiller et al. 2005; Hanson et al. 2010).

3.5. Gas Collection System: Well Properties

The design of gas extraction systems is an essential element for management of large MSW landfills (Fabbricino 2007). Landfill gas operators apply a vacuum of 5 cm to 50 cm of water head in the well, which results in typical gas flow rates less than 25 m^3/hour, equivalent to ~15 standard cubic feet per minute (scfm) at 20°C and 1 atm. T2LBM provides two options to simulate gas extraction. In the first option, the user can specify a fixed mass extraction rate (kg/s) to any desired grid block. By this approach, the grid block will behave as a sink for the specified mass component with the specified rate. The advantage is the simplicity of implementing the extraction rate in the model and thus the straightforwardness in flow rate calculations for a column of grid block sinks (e.g., modeling a single extraction well). On the other hand, the disadvantage is that the extraction rate is a fixed term, which results in two consequences. As mentioned in earlier sections, T2LBM incorporates Monod kinetics to simulate substrate utilization and biomass growth and decay. The biogas generation resulting from this kinetics-controlled biodegradation process will follow a non-linear path. There is no obvious method to match the fixed constant rate of mass extraction specified in the sink grid block(s) with the kinetics-controlled (varying with time) production rate. As a result, the gas pressure could increase or decrease unphysically and out of range of an actual landfill. The other disadvantage of this option is that excessive gas extraction may cause gas-phase disappearance (a situation in an unsaturated model that is physically impossible), which causes non-convergence issues in the simulation.

The alternative option is to utilize the *well on deliverability* model available in TOUGH2. The user can specify a constant vacuum pressure (P_{wb}) for any individual well grid block, and the pressure difference (drawdown) will direct the fluid flow toward these gas well grid blocks at the appropriate rate. The advantage of this option is that non-linear gas production rate will naturally be accommodated by increasing or decreasing the well productivity. Thus, the landfill simulation will more accurately model actual landfill and biogas well extraction behavior. The drawback to this approach is the relative complexity in the design of the well discretization and assignment of parameters for the gas well grid blocks. The heterogeneity of the MSW layers must also be taken into account. If a well is located in multiple layers with different horizontal permeability, different values of the productivity index (PI) should be defined.

In this model landfill system, six (6) gas extraction wells 50 m apart with different slot lengths and extraction rates were modeled. The extraction rate equation is estimated in Eq. (8) for a steady radial flow in layer l:

$$PI_l = \frac{2\pi\left(k\Delta z_l\right)}{\ln\left(r_e / r_w\right) + \left(\frac{s-1}{2}\right)} \tag{8}$$

$$r_e = \sqrt{A / \pi} \tag{9}$$

where Δz_l denotes the layer thickness (slot length of well in each layer), $k\Delta z_l$ is the permeability-thickness product in layer l (see Table 1 for k_x values), r_e is the effective radius of the grid block (see Eq. (9)), r_w is the well radius (12.5 cm for all gas wells), and s is the skin factor (neglected in this study), and A is the connection area (flow cross-section = 2 m^2) of the grid blocks.

The skin factor represents fluid flow restriction that can cause pressure drop near the well, and it can be used as a calibration factor to match measured flow rates (Chen et al. 2021). This parameter was assumed to be unity in the present study making the skin term in Eq. (8) equal to zero. This was considered reasonable because the study is focused on replicating general landfill field conditions, with the intent on performing sensitivity analyses.

The flow rate of fluid phase into the extraction wells is calculated based on Eq. (10) (Pruess et al. 1999), where the extraction wells operate under a pressure differential with P_{wb} serving as the reference well pressure. In this option, the mass production rate of fluid phase (β) from a grid block is estimated in Eq. (10) when the phase pressure $P_\beta > P_{wb}$:

$$q_\beta = \frac{k_{r\beta}}{\mu_\beta} \rho_\beta \; PI \; \left(P_\beta - P_{wb}\right) \tag{10}$$

where $k_{r\beta}$, ρ_β, and μ_β are relative permeability, density and dynamic viscosity of fluid phase β, respectively, and P_β is the pressure of fluid phase β in the grid block(s) adjacent to the grid block at the bottom of the well. Because of the unsaturated nature of this model, the extraction wells in the landfill only collect gas phase generated in the landfill (along with air injected or leaking in from external sources), not the liquid phase. Therefore, the wells are referred to as a "gas collection" system in this model.

The well properties, operational parameters, and spacing of the landfill gas collection system control gas collection efficiency. The choice to use the productivity index option as the basis of the gas collection system design was discussed above. With this choice made, well spacing is critical because of the direct impact of radius of influence (ROI) of the gas wells on the collection efficiency. The ROI is defined as the radial distance that a vertical well can effectively extract landfill gas (US EPA 2017). Vigneault et al. (2004) describe the ROI as the average radial distance from a gas collection well defining a volume within which 90% of the landfill gas generated in the waste is collected at the well, which primarily depends on MSW physical properties, gas generation rate, and pressure (Vigneault et al. 2004). Feng et al. (2017) indicate that the varying physical properties and age of MSW with depth and vacuum pressure are key parameters to consider when designing the well spacing and ROI. Vigneault et al. (2004) show that a vacuum of 4.5 kPa (45 cm of water) results in a radial influence of 33 m at peak methane generation. Feng et al. (2017) indicate that radius of influence is 25 m at a vacuum of 4 kPa (40 cm of water). In the T2LBM model, the 50 m distance between gas wells requires the ROI not to be less than 25 m. Thus, the vacuum of 5 kPa (50 cm of water) was applied to each gas well so that the minimum ROI of 25 m for each gas well is achieved.

3.6. Enthalpy of Reactions

Due to the diversity of MSW composition, many substrates, such as proteins and carbohydrates, can undergo biological biodegradation. In T2LBM, MBSP releases approximately the same heat per mole as that of cellulose. Specifically, anaerobic and aerobic biodegradation of MBSP release

~1.0 and 15 MJ/kg of MBSP, respectively. This approach was also implemented by Hao et al. (2017), where they defined the main heat generation rates arising from aerobic and anaerobic biodegradation of cellulose. The enthalpy of anaerobic and aerobic biodegradation set in the model have direct correlation with maximum heat generation of these reactions which is discussed and compared with heat generated from composted piles in section 5.2.

3.7. Biological Reaction Parameters

T2LBM incorporates Monod kinetics to model the biological reactions. Monod kinetics vary not only for each bacterial species but also for the environment in which bacterial communities are growing. Simplifications must be made to model the highly complex biological processes, and calibrations are needed to tune the overall effect of simplified biodegradation reactions. The kinetic parameters used for each biological reaction are listed in Table S3. Anaerobic biomass yield coefficient (Y), maximum growth rate (μ_{max}), and decay rate (δ) values are within the range of study results by El-Fadel et al. (1997) and Pareek et al. (1999). The yield coefficient of the aerobic biomass is selected from Oldenburg (2001), which were validated against the bench-scale reactor experiments by Kaiser (1996). Sensitivity assessment of input variables is a crucial part of ecological and environmental related numerical simulations (Baharvand et al. 2020; Baharvand and Laskar-Ara 2021). Sensitivity analysis and model calibration were conducted to determine parameter values for which simulation results would fit with the real landfill data. This step of the study developed the initial conditions for further modeling scenarios of air intrusion. The sensitivity analyses were focused on identifying the pertinent biological reaction parameters (listed in Table S3) that controlled the magnitude and time rate of gas production. In the next step, a LandGEM model was developed for the landfill site, which produced a cumulative gas production over 30 years based on incoming waste and air space. The MSW mass of the LandGEM and T2LBM models were normalized to match a gas production curve with LandGEM (see Fig. S3). While in the range reported in the literature, gas collection system performance was expanded based on gas production performance of the model. Sensitivity analyses on parameters listed in Table S2 were conducted such that the gas collection system was performing to metrics reported in the literature.

The critical O_2 concentration in the model was set to 0.18 mg/L (~ 2% v/v in gas phase). The concept of critical O_2 simply means that the aerobic bacteria cannot grow at O_2 concentrations below that value. Different results were reported by various researchers for this value. Aerobic activities were observed at O_2 levels of 1 to 3% v/v (Hale Boothe et al. 2001; Powell et al. 2006), while Yazdani et al. (2010) indicated that even at O_2 levels above 15% the aerobic activity was either not observed or very difficult to achieve at some locations of a aerated MSW landfill cell. Megalla et al. (2016) shows that aerobic activity starts at 2 to 3% v/v and reaches to peak aerobic activity at O_2 level of 9% v/v.

4. DEVELOPMENT OF ANAEROBIC INITIAL CONDITIONS

4.1. Biogas Generation

LandGEM was used to calibrate the anaerobic biological parameters and verify the gas production of the system (Alexander et al. 2005). The conventional value for CH_4 generation constant (k_M) in the non-arid region (0.04 year^{-1}) was selected, along with the potential methane generation capacity (L_o) of 100 m^3/Mg. The case study considers landfilled ~15 million Mg over 8 years. To compare LandGEM gas generation to T2LBM, the gas generation rates were normalized to the Mg of waste in each respective model. For example, the T2LBM model consists of 12,000 Mg of MSW (volume per grid block × bulk density of MSW × number of grid blocks). As a result, gas generation was modeled to replicate the LandGEM gas production such that the maximum biogas was generated over the first 8 years and the rate of biodegradation exponentially decreased over the next 50 years. The cumulative biogas production in Fig. S3 represents the six gas wells over the ~60 years of operation.

4.2. Gas Collection System Performance

The parameters r_e, r_w, and s in Eq. (8). were fit and listed in Table S2 such that the gas extraction flow rates range between 1.7 to 34 m^3/min and the ROI of adjacent wells overlap (i.e., ROI is at least 50 m). This design basis and related sensitivity analyses led us to assign the specified values for each well at different layers in Table S2. The gas collection wells typically operate with a controllable vacuum, where the gas flow rates range from 0 to 25 m^3/hour (0 to 15 scfm) depending on the screen length and location. Thus, the proper PI and P_{wb} were assigned to the gas wells to reflect this range of gas extraction. In particular, Fig. S4 shows gas wells GW-3 and GW-4 extract the most biogas, peak of 6 m^3/yr/Mg MSW after ~5 years before exponentially decreasing to less than 3 m^3/yr/Mg MSW after ~20 yrs. In contrast, the gas wells GW-1, 2, 5, and 6 collect less than 1 m^3/yr/Mg MSW. Thus, the majority of the gas extraction stems from the central two gas wells. The total gas extraction rate peaks at 14 m^3/yr/Mg MSW (~11 scfm) after ~5 yrs.

4.3. Temperature and Pressure

Fig. 2 shows the spatial and temporal changes in temperature and pressure with the onset of anaerobic decomposition. In particular, Fig. 2(a) shows that the maximum temperature occurs within the middle third of the landfill after year 5. Fig. S5 shows temperature contour plots for the landfill at years 1, 5, 15, and 30, which are parabolic with the maximum temperature in the middle depth. The atmosphere and underlying soil below the composite liner system serve as heat sinks. Fig. 2(b) shows the gas pressure remains constant with depth until it reaches the lowest MSW layer. The vectors in Fig. 2(b) correspond to the direction and magnitude of gas flowing to the gas extraction wells. For example, the shallow layer exhibits the most gas flow, collected by GW-3 and GW-4, because of the lower hydraulic conductivity and less decomposition. This implies that slot lengths extending closer to the surface could be an effective tool in collecting high methane yields in shallow layers. The performance of each gas collection well is shown in Fig. S4, where the maximum gas collection is occurring at year 5.

In Fig. 2(c), the modeled landfill temperatures are presented 1, 5, 15, 20, and 30 years after initiating the simulation. Landfill temperatures are simulated for 60 years for anaerobic biodegradation, but the temperature is constant after 30 years. Although the inhibiting temperature for anaerobic biodegradation is assumed to be 65°C and above, the temperature reaches to a maximum value of 60°C after 6 years which is dependent on anaerobic heat generation rate, moisture content, available substrate, and thermo-physical properties of MSW. At 6 years, the gas generation rate is also at its maximum, and the gas collection system is operating at its highest recovery rate (see Eq. 10). The temperatures are spatially distributed such that the middle third of the landfill is warmest and coolest at the surface cover system-atmosphere boundary, which aligns with the results of Hanson et al. (2010). The temperature profile after 15 years indicates that heat generation from anaerobic microbial activity is decreasing after reaching the peak of microbial activity, resulting in lower temperatures compared to year 5 because of heat loss through the top boundary. The temperature decreases to 45°C in the center of the landfill after 30 years.

The temporal variation of landfill gas pressures in Fig. 2(d) are obtained from the center line in Fig. 2(b). Gas pressures increase concomitantly with increasing gas production, from atmospheric pressure at the start of simulations to 35 kPa at year 5. At peak gas production (year 5), the gas pressure is 36 kPa, and it decreases to 8 kPa by year 30. This suggests that excess gas pressures exist even though the gas wells are extracting gas at a vacuum of 5 kPa. The gas pressure is constant along the depth of shallow and intermediate MSW layers, but it increases with depth in the deep MSW layer. This is likely attributed to the degree of saturation increasing the deep layer towards the leachate level and thus inhibiting gas transport (i.e., build up occurs).

5. RESULTS AND DISCUSSION OF AIR INTRUSION

5.1. Scenario 1: Air intrusion through interim clay cover system.

Scenario 1 is focused on air intrusion occurring through cracks in the daily and interim soil cover layer. Landfill methane emissions depend on several factors, e.g., cover soils, gas collection efficiency, changes in barometric pressure, etc.; rising barometric pressure suppressed the emission, while falling barometric pressure enhances the emission (Bogner et al. 2011; Xu et al. 2014; Young 1990, 1992). In Scenario 1, this barometric pumping is overcome by the pressure differential between the landfill and atmosphere from the gas extraction wells, especially on side slopes with nearby gas wells where landfill capping is not as easily compacted (Di Trapani et al. 2013). This results in air ingress and a rapid aerobic conversion of the MSW with temperatures rising in a few days. One month of air ingress was selected to reflect the time-elevated concentrations of O_2 and N_2 that are anecdotally observed in gas wells. Simulation results in Fig. S8(a) show the landfill operating under a steady anaerobic condition with average temperature profiles reported in Fig. 2. Air intrusion occurs because of a pressure differential of 5 kPa combined with a single grid block of the clay cover simulated as a high-permeability material to reflect a crack. This leads air flowing into MSW with rate of 0.34 m^3/hour (0.2 scfm). In Fig. S8(b), the temperature rapidly rises to 80°C after 1 month of air ingress. The surrounding region impacted by air intrusion and thus aerobic reactions is localized to less than 10m into the waste, with O_2 completely consumed at the entrance location. In contrast, the N_2 penetrates deeper into the landfill, which could explain why N_2 is observed in gas wells with limited corresponding O_2. In Fig. S8(c), the temperature decreases to 60°C after 1 month as the system returns to anaerobic conditions. This may be attributed to the small impacted region and heat transfer to the surrounding waste and to the atmosphere. Temperature approach normal conditions in Fig. S8(d) after 1 year.

The spatial distribution of gas composition in Fig. 3 is compared after the first week and after 1 month of air intrusion. In particular, N_2 progresses ~50 m into the shallow MSW layer and only 10 m in the intermediate MSW layer after 1 week. The lower permeability of the intermediate layer explains the significantly lower penetration of N_2. After 1 month, N_2 extends farther into the waste mass (approximately 100 m and 50 m into the shallow and intermediate layers, respectively), where it intersects with the GW2 and GW3 extraction wells. Oxygen remains localized during the intrusion because of the high aerobic biodegradation activity of the waste, meaning that O_2 consumption relies on the availability of biodegradable substrates, critical O_2 for aerobic biodegradation, and the number of aerobic bacteria. As a result, the simulations indicate that high aerobic activity at the location of intrusion consume all of the O_2 entering into MSW and simultaneously 40% water vapor is produced as the result of high aerobic biodegrading. The CH_4 and CO_2 concentrations in the landfill decrease instantly at the onset of air intrusion. After 1 month of air intrusion, CH_4 level drops significantly and CO_2 concentrations increase to ~15%. If CO_2 concentration were only controlled by the aerobic reaction, the concentration by volume of the gas phase would be approximately 50%. The fact that the CO_2 concentration only reaches 15% confirms that the CO_2 levels are a product of aerobic biodegradation and air ingress.

In Fig. S9(a), the time-history of biogas production is compared before and after air intrusion. The simulations indicate that the maximum biogas remaining in the system is 2,400 m^3 6 years after the landfill closure. The air intrusion occurs 30 years after the closure and continues for 1 month. During the air intrusion, CO_2 and CH_4 concentrations in the biogas concurrently decrease but not equally. For example, the CO_2 volume in the biogas decreases from 1,800 m^3 to 1,500 m^3 (at temperature and pressures inside the landfill), whereas the CH_4 volume reduces to 1200 m^3. Fig. S9(a) confirms that the higher CO_2 production is related to aerobic biodegradation. Air injection experiments by Powell et al. (2006) also show the reduction in CH_4 concentration is attributed to a combination of presence of air and inhibition of anaerobic biodegradation. The simulation results in Fig. S9(b) also indicate that more than one year was required after the repair of the air intrusion to re-establish normal anaerobic conditions.

5.2. Scenario 2: Air leakage from an air line break.

Scenario 2 involves simulating air ingress from air line breaks. These air lines are installed below the soil cover system in the waste mass, and they are used to provide air pressure to operate the pneumatic pumps removing liquids from gas extraction wells. The air lines can become buried deeper into the landfill as waste lifts are added over time, which is why in Scenario 2 the air line break was placed at the interface between shallow and intermediate MSW layers. The air lines contain atmospheric air pressurized to approximately 500 kPa (73 psi). Although rare, the air line may break because of differential settlement and reduced service life of the HDPE piping. An air line break was simulated by applying a constant mass flow rate of 2.58×10^{-3} kg/s and 7.3×10^{-4}

kg/s for N_2 and O_2, respectively. This is approximately equal to 11.9 m^3/hour (7 scfm) of air flow rate injecting into the MSW. The leakage occurs in a grid block at the interface of the shallow and intermediate MSW layers, located at the depth of 17 m. As previously stated, the air line leak included in this study was based loosely on an actual air line leak event at an MSW landfill in the southern US. The input parameters (such as line diameter, flow rate, and generalized depth) were obtained from field personnel associated with the landfill operation.

Similar to Fig. S8(a), the landfill is operating under anaerobic conditions prior to the air line break in Fig. 4(a). After the onset of the air line break, it is assumed that the air line break is repaired after 1 week. The landfill temperatures rise to 80°C in that timeframe, quicker than was observed in Scenario 1. Based on Fig. 4(b), the area of heat generation is approximately 50 m wide and approximately 5 times greater than the area of influence in Scenario 1. This is attributed to a higher air-injection flowrate from the pressurized air line. After the air line is repaired, Fig. 4(c) implies that the heat accumulation region remains at 80°C after 1 month. The simulation results in Fig. 4(d) indicate that temperatures still remain elevated (~60°C) one year after the air line break. This suggests that heat generated by the reactions stimulated by an air line break can persist for a long time, which can facilitate other chemical reactions, impact methane energy recovery, and performance of geosynthetics (Jafari et al. 2014, 2017). The maximum heat flux produced by the anaerobic reactions in this model is approximately 2 W/m^3. In contrast, the maximum heat flux increases to ~500 W/m^3 in the aerobic scenario.

Due to aerobic heat generation, the degree of water (aqueous phase) saturation also dramatically changes at the air line break. In Fig. 5, the degree of saturation decreases from over 30% to 10% at the boundary between the shallow and intermediate layers, which also corresponds to the zone of heat accumulation. The temperature profile shows that the higher temperatures are predominantly in the shallow layer between the depths 10 m to 18 m. This is attributed to the higher permeability of shallow layers facilitating heat conduction and gas transport. Thus, more O_2 is available to the aerobic microorganisms located in the shallow layer, and additional aerobic biodegradation will result in temperature increase and moisture redistribution in a wider region.

The spatial distribution of gas composition from Scenario 2 in Fig. S10 compares gas composition after one week of the broken air line and one year after the repair. During the air line break, air reaches the interim soil cover due to the relatively high mass flow rate and permeability of the shallow MSW layer, impacting a region that is 150 m wide. Effective gas capture at the surface of the landfill becomes a vital operation in this scenario to avoid ballooning of gas under an exposed geomembrane at the landfill surface as a result of gas migration to the surface (Townsend et al. 2015b). Oxygen concentration at the air line break is ~12% v/v and decreases to 5% v/v at the interim soil cover. At the center of the aerobic reactions, the gas composition is 8% v/v O_2 and 50% v/v N_2, with the remaining gas composed of 42% v/v water vapor. The ratio of N_2 to O_2 is correspondingly 6.25, which is significantly higher than 3.76 for air. This implies that increasing N_2 to O_2 ratios signify consumed O_2 from aerobic reactions. The excessive O_2 concentration is observed because of the imbalance between the O_2 consumption rate by aerobic bacteria and injection rate from pressurized air line. After the air line is repaired, traces of $N_2$are found at the top of the landfill. The CH_4 and CO_2 concentrations are almost fully recovered after 1 year of the air line break, and there is no O_2 remaining in the landfill.

Depending on the mass balance between air injection rate (and duration) and rapid oxygen consumption rate during aerobic biodegradation at the injection location, oxygen could transfer to the adjacent grid blocks and create a larger area of aerobic impact. Each grid block receives various amounts of oxygen at any time and hence generates various amounts of heat. As an illustrating example, input parameter values were considered for air injection rate = 18 m^3/hour (10.4 scfm), horizontal permeability k_x = 3.75×10^{-11} m^2, specific heat capacity C_p =1000 J/kg·K. Results showed that after 2 days of injection the aerobic zone was 12 m^2. After 7 days of injection, 250 grid blocks experienced aerobic reactions and the area increased to 500 m^2. To better understand the amount of heat generated inside the aerobic zone, the grid blocks exhibiting aerobic activity and temperature above 75°C were identified and compiled first. To calculate the amount of aerobic heat generated to cause a temperature change, with the assumptions that the fluid pressure remains constant within the one week of injection and solid-fluid phase change temperature together, Eq. (11) was used to calculate aerobic heat of enthalpy:

$$Q = \left[(1-n)(\rho_s \cdot C_s) + n(\rho_g \cdot C_g + \rho_l \cdot C_l)\right]\Delta T \tag{11}$$

where Q is expressed as kJ/m^3, n is porosity, ρ is density, C is specific heat capacity, ΔT is temperature change during each time step of simulation, and *s, g*, and *l* stand for solid, gas, and liquid phase, respectively. To calculate the amount of heat flux generated by each cell, Eq. (12) was used:

$$q = \frac{Q}{\Delta t} \tag{12}$$

where q is expressed as W/m^3, and Δt is the simulation time step. Presented in Fig. 6, the (1) temperature, (2) heat of enthalpy, and (3) heat flux at grid blocks located at the injection location, along with 10 m and 30 m to the left side of it. At the injection location, the temperature increases by 30°C but at a slower rate (3 to 4 days) because of the cooling effect of injected air temperature (25°C). Temperature increased by 35°C within 1 day at the 10 m and 30 m left of the injection point. The aerobic reaction generated 200-250 kJ/m^3 of heat of enthalpy, equivalent to 400-500 W/m^3 of heat flux inside the individual grid blocks (if considering the third dimension of each grid block to be 1 m into the page).

To calculate the average heat flux generated by each individual grid block, the area under dashed line was divided by the time of occurrence. For example, for the 30 m grid block, the area under dashed line was ~ 360 W·day/m^3 which divided by 2 days of heat generation (day 4.5 to day 6.5), an estimation of 180 W/m^3 as the average heat flux was resulted. The same approach was used to calculate the average heat flux of each grid block inside of the aerobic zone, and were summed and averaged within all the grid blocks. Results are shown in Fig. S11 for four (4) air flow rates.

Fig. 7 shows the correlation between aerobic zone, average heat flux, specific heat, horizontal permeability, and air flow. In this figure, the aerobic zone was reported after 7 days of air injection. Based on the sensitivity analysis, the heat flux and aerobic zone non-linearly rise with increasing air flow, coming to an asymptote at the higher air flow rates. When C_p increases from 1,000 to 3,000 J/kg·K, the area also increases by a factor of 3. The effect of C_p is less pronounced with heat flux, where a higher C_p corresponds to slightly higher heat flux. The sensitivity analysis confirms that a higher C_p corresponds to a waste with more capacity to accumulate heat before the temperatures increases. Results in Fig. 7 indicate that heat generation rates increase linearly to 8.5 m^3/hour (~5 scfm) before approaching an asymptote at 140 W/m^3. The heat generation is also relatively equal over the range of C_p, which signifies that the aerobic reactions are independent of physical properties. The air flow rate of 0.34 m^3/hour (0.2 scfm) corresponding to scenario 1 results in an aerobic zone area of less than 20 m^2 and heat generation rate of ~20 W/m^3. The latter is close to the results of Megalla et al. (2016), where the maximum heat generation from aerobic heat generation from surface air intrusion was reported 44.6 W/m^3 and is comparable to values measured in aerobic composting piles (Zambra et al. 2011). In contrast, the air flow rate of 11.9 m^3/hour (7 scfm) from scenario 2 corresponds to heat generation of 100 W/m^3 and an aerobic area of 250 m^2. While the C_P does not influence heat generation, it plays a major role in the formation of the aerobic zone. For example, a C_P of 1,000 J/kg·K corresponds to area of 200 m^2 at an air flow of 5 scfm, compared to 140 m^2 and 60 m^2 for heat capacities of 2,000 J/kg·K and 3,000 J/kg·K, respectively. This trend is observed because the heat generated from aerobic reactions is first used to raise the waste temperature, which requires more at higher C_P (e.g., 3,000 J/kg·K). Therefore, the additional heat available for 1,000 J/kg·K can propagate further outward from the air line break and raise the temperature of adjacent waste.

Heat generation rate values above 100 W/m^3 may perhaps be beyond of available published data. This output stems from the TOUGH code, where the multiphase and multiphysics processes have been previously verified and validated (Jung et al. 2010; Kling and Korkealaakso 2006; Nastev et al. 2001; Oldenburg et al. 2002; Pruess 2004; Vigneault et al. 2004). The simulations performed and reported herein are within the constraints of TOUGH capabilities. Moreover, it is important to report possible upper bound heat generations as worst-case scenario when excess aeration/air intrusion incidents occur.

6. PRACTICAL IMPLICATIONS

The solid waste industry faces many challenges, including a better understanding of the cause of significant changes in temperatures within the waste mass (other than normal anaerobic decomposition heat) and control of greenhouse gas emissions to the atmosphere under ever restrictive regulations. At a minimum, standard operational practice for control of emissions includes the effective extraction of landfills gas, especially during interim stages of operation where a final cover system is not in place. Well field tuning is a common operation and management (O&M) task that optimizes gas extraction while not overpulling on each individual gas well. Historical practice limits overpulling on a gas well to prevent air flow into the waste mass through the interim cover system and cause a landfill fire. As a result, standard gas well design includes use of solid pipe (with no slots) in the upper 6 m to 9 m (20 to 30 ft) of pipe from top of waste (e.g., Fig. 1 red slots in the gas wells) such that application of a vacuum is limited in the upper-most portion of the waste mass, and installation of a bentonite plug at the waste/soil interface to prevent potential air intrusion. When the interim cover is less than optimal, the potential result of localized higher concentration of methane emissions are possible, a concern where emissions are more tightly controlled by regulation.

Scenario 1 in this T2LBM modeling study indicated that the pulling of atmospheric oxygen into the waste mass by the gas well could cause heat accumulation due to aerobic reactions near the landfill side slope (Fig. S8). However, this localized volume (that is flux) of oxygen is not sufficient to cause an exothermic reaction beyond the proximity to the well bore. For a larger-scale exothermic event to occur due to aerobic reactions, a larger flux of air (such as an air line break) is required to increase heat generation rates (Fig. 7). This observation is important to the solid waste industry, as it could revise gas well design and allow slotted pipe to be located closer to the top of waste. This correspondingly could facilitate improved methane collection in shallower waste layers (see large vectors pointed toward GW-3 and GW-4 in Fig. 2(b) in the shallow MSW layer) and hence improved productivity for renewable energy plants, as long as the vacuum applied to the well is optimized to limit air intrusion. This theory from modeled results needs to be field verified across multiple landfills to demonstrate reproducibility before a broad application of the results are implemented. Moreover, comprehensive numerical sensitivity analyses should be performed considering interim cover system, leachate and gas pressures, waste decomposition stage and composition, landfilling history, climate conditions, among many factors.

Secondary implications of aerobic reactions from the T2LBM model include higher temperatures impacting geosynthetic components in drainage systems (specifically horizontal and vertical gravity drainage pipes) and accelerated decomposition leading to differential settlement. In particular, temperatures from 70 to 80°C can reduce the elastic modulus of the pipe (Bilgin et al. 2007) and accelerate antioxidant completion and thus reduce the time to stress cracking of high-density polyethylene (HDPE) (Hsuan and Koerner, 1998), which can dramatically reduce the service life and efficacy of internal drainage pipes within the waste mass. While this condition was not modeled, the technical opinion that even localized air intrusion could result in damage to the integrity to HDPE piping systems is reasonable and should be considered by the industry in design and operation of gas extraction systems.

Monitoring of signs of pre-cursors to an exothermic event, in this case from air intrusion, is important to the industry. In addition to the monitoring of oxygen in gas wells, visual inspections designed to identify unexplained differential settlement should be part of the routine O&M activities at an MSW landfill. Accounting for differential landfill settlement caused by aerobic decomposition could be important for operation of the landfill gas extraction system, i.e., necessary for the piping to be graded such that condensate cannot collect in low spots and block the flow of landfill gas. While limited settlement data is available, field monitoring of aerobic landfill cells suggest that the magnitude of settlement is relatively similar to leachate recirculation but likely at a quicker rate (Mehta et al. 2002; Yazdani et al. 2006; Merz and Stone 1962; Borglin et al. 2004).

This implies that regions impacted by subsurface air line breaks could experience rapid differential settlement, which could correspondingly serve as a lagging indicator of an air line break. Routine operation and maintenance inspections could be implemented to check the integrity of air lines and gas header pipes as mitigation measures.

7. CONCLUSIONS

The prediction of heat generation and temperature increase, along with changes in gas composition and concentration, as result of air intrusion are provided in this study using T2LBM. The model incorporated aerobic and anaerobic biodegradation processes, heat generation, and fluid transfer. The model geometry, layering, material properties, and gas extraction were developed based on a landfill in the Midwestern U.S. The model was qualitatively calibrated by using trends in field temperature profiles and biogas production rates from LandGEM. Air intrusion through the cover system and air leakage from air line system were simulated to investigate the impact of air intrusion into MSW landfill. The effect of air intrusion on biodegradation processes, along with subsequent change in heat generation and gas composition in the landfill were presented. The following conclusions are inferred from the numerical simulation results in this study:

Aerobic biodegradation releases a heat flux of 10 to 140 W/m^3 depending on the rate of air flow, which rapidly causes the waste temperature in the vicinity of the reactions to increase up to 80°C. Similar heat generation fluxes are attainable when low air flow rates intrude into the waste mass, as compared with compost piles. Field investigations are needed to document the air line flow rates to corroborate this study. The rapid rate of O_2 consumption by aerobic microbes near the point of entry hinders O_2 transport (penetration) farther into the waste mass, which correspondingly limits the impacted area to less than 10 m near the cracked interim soil cover.

Moreover, heat conduction from MSW towards the atmosphere causes the temperature to decrease to less than 60°C a few months after the air intrusion is ceased. For scenario 2 air line break, the zone of heat accumulation remains elevated above baseline for normal biochemical waste degradation for 12 months after the air line is repaired, negatively impacts the settlement and methane generation rates. A high flux infusion of O_2 in an air line break can facilitate exothermic reactions and therefore should be a key focus from the solid waste industry in their efforts to prevent heat accumulations. However, the simulations were performed assuming MSW as a homogeneous material in each layer. This is not the case and hence the simulation results likely represent a conservative estimate on the zone of heat accumulation.

The oxygen concentration varies spatially after entering into the landfill. Oxygen consumption is controlled by aerobic bacteria concentration, critical O_2 concentration, O_2 intrusion rate, temperature, moisture content, and Monod kinetic parameters. The ratio of N_2 to O_2 increases from 3.76 for atmospheric air to higher values depending on the rate of air intrusion. The ratio of CH_4 to CO_2 starts at unity for anaerobic decomposition, but air intrusion causes a decrease due to a combination of the presence of air replacing CH_4 and CO_2 and inhibition of anaerobic biodegradation. At the same time, aerobic biodegradation produces CO_2 as a byproduct. Thus, a signal of aerobic decomposition for landfill operators is not only the decrease in the ratio of CH_4 to CO_2 but also relative increase in CO_2 flow rate.

The lower vertical permeability compared to horizontal, causes the air to flow further laterally and therefore the heat accumulation zone forms an elliptical area that can be quantified in Fig. 7. The elliptical aerobic area is influenced by the air flow rate and specific heat capacity, higher heat capacity corresponding to smaller heat accumulation zones. Results from this study helps practitioners to estimate the magnitude and area of impact of the aerobic transition. However, the simulated heat accumulation zones are likely a conservative prediction because the MSW was considered as a homogeneous material.

ACKNOWLEDGMENTS

The authors wish to acknowledge the resources and data provided by Waste Management in assist in the development and calibration of the model. Any opinions, findings, conclusions, or recommendations expressed in this material are those of the author(s) only and do not necessarily reflect the views of Waste Management. The assistance of the research group members, specifically Jack Cadigan and William Ard, are greatly appreciated.

Nomenclature

Letters			
A	Area	w	Gravimetric moisture content
B	Bacteria (Biomass)	x	Horizontal
BA	Aerobic bacteria	Y	Yield coefficient
BN	Anaerobic bacteria	z	Vertical
C_p	Specific heat capacity		
f	Coefficient of temperature dependent growth	*Greek symbols*	
g	Gravity	μ	Growth rate
K	Hydraulic conductivity	δ	Death rate
K_T	Thermal conductivity	ρ	Density
k	Intrinsic permeability	σ	Stress
k_r	Relative permeability	β	Fluid
n	Porosity	η	Dynamic viscosity
P	Pressure		
q	Flow rate	*Subscript*	
r_e	Effective radius of grid block	T	Temperature
r_w	Well radius	w	Water

S	Substrate	*v*	Vertical
T	Temperature	*wb*	Wellbore
t	Time		

REFERENCES

Alexander, A., Burklin, C., & Singleton, A. (2005). *Landfill Gas Emissions Model (LandGEM) Version 3.02 User's Guide*. *May*, 56. https://www3.epa.gov/ttn/catc/dir1/landgem-v302-guide.pdf

Assessment of the Performance of Engineered Waste Containment Barriers. (2007). National Academies Press. https://doi.org/10.17226/11930

Baharvand, S., Jozaghi, A., Fatahi-Alkouhi, R., Karimzadeh, S., Nasiri, R., & Lashkar-Ara, B. (2020). Comparative Study on the Machine Learning and Regression-Based Approaches to Predict the Hydraulic Jump Sequent Depth Ratio. *Iranian Journal of Science and Technology - Transactions of Civil Engineering*, *0123456789*. https://doi.org/10.1007/s40996-020-00526-2

Baharvand, S., & Laskar-Ara, B. (2021). Hydraulic design criteria of the modified meander C-type fishway using the combined experimental and CFD models. *Ecological Engineering*, *164*(March), 106207. https://doi.org/10.1016/j.ecoleng.2021.106207

Beaven, R. P. (2000). *The hydrogeological and geotechnical properties of household waste in relation to sustainable landfilling*. *January*. http://qmro.qmul.ac.uk/jspui/handle/123456789/1698

Bilgin, Ö., Stewart, H. E., & O'Rourke, T. D. (2007). Thermal and Mechanical Properties of Polyethylene Pipes. *Journal of Materials in Civil Engineering*, *19*(12), 1043–1052. https://doi.org/10.1061/(ASCE)0899-1561(2007)19:12(1043)

Bogner, J. E., Spokas, K. A., & Chanton, J. P. (2011). Seasonal Greenhouse Gas Emissions (Methane, Carbon Dioxide, Nitrous Oxide) from Engineered Landfills: Daily, Intermediate, and Final California Cover Soils. *Journal of Environmental Quality*, *40*(3), 1010–1020. https://doi.org/10.2134/jeq2010.0407

Borglin, S. E., Hazen, T. C., Oldenburg, C. M., & Zawislanski, P. T. (2004). Comparison of aerobic and anaerobic biotreatment of municipal solid waste. *Journal of the Air and Waste Management Association*, *54*(7), 815–822.

https://doi.org/10.1080/10473289.2004.10470951

Breitmeyer, R. J., & Benson, C. H. (2014). Evaluation of parameterization techniques for unsaturated hydraulic conductivity functions for municipal solid waste. *Geotechnical Testing Journal*, *37*(4). https://doi.org/10.1520/GTJ20130132

Breitmeyer, R. J., Benson, C. H., & Edil, T. B. (2019). Effects of Compression and Decomposition on Saturated Hydraulic Conductivity of Municipal Solid Waste in Bioreactor Landfills. *Journal of Geotechnical and Geoenvironmental Engineering*, *145*(4), 1–15. https://doi.org/10.1061/(ASCE)GT.1943-5606.0002026

Calder, G. V., & Stark, T. D. (2010). Aluminum reactions and problems in municipal solid waste landfills. *Practice Periodical of Hazardous, Toxic, and Radioactive Waste Management*, *14*(4), 258–265. https://doi.org/10.1061/(ASCE)HZ.1944-8376.0000045

Chen, Y.-H., Tsai, F. T.-C., & Jafari, N. H. (2021). Multiobjective Optimization of Relief Well Operations to Improve Levee Safety. *Journal of Geotechnical and Geoenvironmental Engineering*, *147*(7), 1–17. https://doi.org/10.1061/(asce)gt.1943-5606.0002532

De la Cruz, F. B., Cheng, Q., Call, D. F., & Barlaz, M. A. (2021). Evidence of thermophilic waste decomposition at a landfill exhibiting elevated temperature regions. *Waste Management*, *124*, 26–35. https://doi.org/10.1016/j.wasman.2021.01.014

Di Trapani, D., Di Bella, G., & Viviani, G. (2013). Uncontrolled methane emissions from a MSW landfill surface: Influence of landfill features and side slopes. *Waste Management*, *33*(10), 2108–2115. https://doi.org/10.1016/j.wasman.2013.01.032

El-Fadel, M., Findikakis, A. N., & Leckie, J. O. (1997). Numerical Modelling of Generation and Transport of Gas and Heat in Sanitary Landfills Iii. Sensitivity Analysis. *Waste Management & Research*, *15*(1), 87–102. https://doi.org/10.1177/0734242x9701500107

Fabbricino, M. (2007). Evaluating operational vacuum for landfill biogas extraction. *Waste Management*, *27*(10), 1393–1399. https://doi.org/10.1016/j.wasman.2006.10.006

Faitli, J., Magyar, T., Erdélyi, A., & Murányi, A. (2015). Characterization of thermal properties of municipal solid waste landfills. *Waste Management*, *36*, 213–221. https://doi.org/10.1016/j.wasman.2014.10.028

Feng, S. J., Zheng, Q. T., & Xie, H. J. (2017). A gas flow model for layered landfills with vertical extraction wells. *Waste Management*, *66*, 103–113. https://doi.org/10.1016/j.wasman.2017.05.001

Gholamifard, S., Eymard, R., & Duquennoi, C. (2008). Modeling anaerobic bioreactor landfills in methanogenic phase: Long term and short term behaviors. *Water Research*, *42*(20), 5061–5071. https://doi.org/10.1016/j.watres.2008.09.040

Hale Boothe, D. D., Smith, M. C., Gattie, D. K., & Das, K. C. (2001). Characterization of microbial populations in landfill leachate and bulk samples during aerobic bioreduction. *Advances in Environmental Research*, *5*(3), 285–294. https://doi.org/10.1016/S1093-0191(00)00063-0

Hanson, J. L., Liu, W. L., & Yesiller, N. (2008). Analytical and numerical methodology for modeling temperatures in landfills. *Geotechnical Special Publication*, *177*, 24–31. https://doi.org/10.1061/40970(309)3

Hanson, J. L., Yeiller, N., & Oettle, N. K. (2010). Spatial and temporal temperature distributions in municipal solid waste landfills. *Journal of Environmental Engineering*, *136*(8), 804–814. https://doi.org/10.1061/(ASCE)EE.1943-7870.0000202

Hao, Z., Barlaz, M. A., & Ducoste, J. (2020). Finite element modeling of landfills to estimate heat generation, transport, and accumulation. *Journal of Geotechnical and Geoenvironmental Engineering*, *146*(12), 1–13. https://doi.org/10.1061/(ASCE)GT.1943-5606.0002403

Hao, Z., Sun, M., Ducoste, J. J., Benson, C. H., Luettich, S., Castaldi, M. J., & Barlaz, M. A. (2017). Heat Generation and Accumulation in Municipal Solid Waste Landfills. *Environmental Science and Technology*, *51*(21), 12434–12442. https://doi.org/10.1021/acs.est.7b01844

Hartz, K. E., Klink, R. E., & Ham, R. K. (1982). Temperature effects: methane generation from landfill samples. *J. Environ. Eng. Div., ASCE;(United States)*, *108*.

Hashemi, M., Kavak, H. I., Tsotsis, T. T., & Sahimi, M. (2002). Computer simulation of gas generation and transport in landfills - I: Quasi-steady-state condition. *Chemical Engineering Science*, *57*(13), 2475–2501. https://doi.org/10.1016/S0009-2509(02)00142-2

Haug, R. T. (2018). *The Practical Handbook of Compost Engineering*. Routledge. https://doi.org/10.1201/9780203736234

Hsuan, Y. G., & Koerner, R. M. (1998). Antioxidant Depletion Lifetime in High Density Polyethylene Geomembranes. *Journal of Geotechnical and Geoenvironmental Engineering*, *124*(6), 532–541. https://doi.org/10.1061/(asce)1090-0241(1998)124:6(532)

Jafari, N. H., Stark, T. D., & Roper, R. (2014). Classification and reactivity of secondary aluminum production waste. *Journal of Hazardous, Toxic, and Radioactive Waste*, *18*(4), 1–11. https://doi.org/10.1061/(ASCE)HZ.2153-5515.0000223

Jafari, N. H., Stark, T. D., & Rowe, R. K. (2014). Service life of HDPE geomembranes subjected to elevated temperatures. *Journal of Hazardous, Toxic, and Radioactive Waste*, *18*(1), 16–26. https://doi.org/10.1061/(ASCE)HZ.2153-5515.0000188

Jafari, N. H., Stark, T. D., & Thalhamer, T. (2017). Progression of elevated temperatures in municipal solid waste landfills. *Journal of Geotechnical and Geoenvironmental Engineering*, *143*(8), 1–16. https://doi.org/10.1061/(ASCE)GT.1943-5606.0001683

Jain, P., Powell, J., Townsend, T. G., & Reinhart, D. R. (2006). Estimating the Hydraulic Conductivity of Landfilled Municipal Solid Waste Using the Borehole Permeameter Test. *Journal of Environmental Engineering*, *132*(6), 645–652. https://doi.org/10.1061/(asce)0733-9372(2006)132:6(645)

Jung, Y., Imhoff, P. T., Don C. Augenstein, & Yazdani, R. (2010). design of settling tanks using CFD. *Policy*, *1*(June), 2010–2010. https://doi.org/10.1061/(ASCE)0733-9372(2009)135

Kaiser, J. (1996). Modelling composting as a microbial ecosystem: A simulation approach. *Ecological Modelling*, *91*(1–3), 25–37. https://doi.org/10.1016/0304-3800(95)00157-3

Kaiser, J., & Soyez, K. (1990). Simulation der aeroben Rotte mit biotechnischen Modellen. *Biologische Verfahren Der Abfallbehandlung, EF, Berlin*, 147–156.

Kasali, G. B., Senior, E., & Watson-Craik, I. A. (1989). Sodium bicarbonate effects on the anaerobic digestion of refuse. *Journal of Chemical Technology & Biotechnology*, *45*(4), 279–289. https://doi.org/10.1002/jctb.280450405

Kavazanjian, E., Matasovic, N., Bonaparte, R., & Schmertmann, G. R. (1995). Evaluation of MSW properties for seismic analysis. *Geotechnical Special Publication*, *46 /2*, 1126–1141.

Klein, R., Baumann, T., Kahapka, E., & Niessner, R. (2001). Temperature development in a modern municipal solid waste incineration (MSWI) bottom ash landfill with regard to sustainable waste management. *Journal of Hazardous Materials*, *83*(3), 265–280. https://doi.org/10.1016/S0304-3894(01)00188-1

Klein, R., Nestle, N., Niessner, R., & Baumann, T. (2003). Numerical modelling of the generation and transport of heat in a bottom ash monofill. *Journal of Hazardous Materials*, *100*(1–3), 147–162. https://doi.org/10.1016/S0304-3894(03)00101-8

Kling, T., & Korkealaakso, J. (2006). Multiphase Modeling and Inversion Methods for Controlling a Landfill Bioreactor. *Tough Symposium 2006*, *1992*.

Lay, J. J., Li, Y. Y., & Noike, T. (1998). Dynamics of methanogenic activities in a landfill bioreactor treating the organic fraction of municipal solid wastes. *Water Science and Technology*, *38*(2), 177–184.

Megalla, D., Van Geel, P. J., & Doyle, J. T. (2016). Simulating the heat budget for waste as it is placed within a landfill operating in a northern climate. *Waste Management*, *55*, 108–117. https://doi.org/10.1016/j.wasman.2015.11.049

Mehta, R., Barlaz, M. A., Yazdani, R., Augenstein, D., Bryars, M., & Sinderson, L. (2002). Refuse Decomposition in the Presence and Absence of Leachate Recirculation. *Journal of Environmental Engineering*, *128*(3), 228–236. https://doi.org/10.1061/(asce)0733-9372(2002)128:3(228)

Merz, R. C., & Stone, R. (1962). Landfill settlement rates. *Public Works*, *93*(9), 103–106.

Moisture Retention Properties of Municipal Solid Waste in Relation to Compression. (2006). *Journal of Geotechnical and Geoenvironmental Engineering*, *132*(10), 1250–1261. https://doi.org/10.1061/(ASCE)1090-0241(2006)132:10(1250)

Narode, A., Pour-Ghaz, M., Ducoste, J. J., & Barlaz, M. A. (2021). Measurement of heat release during hydration and carbonation of ash disposed in landfills using an isothermal calorimeter. *Waste Management*, *124*, 348–355. https://doi.org/https://doi.org/10.1016/j.wasman.2021.02.030

Nastev, M., Therrien, R., Lefebvre, R., & Geélinas, P. (2001). Gas production and migration in landfills and geological materials. *Journal of Contaminant Hydrology*, *52*(1–4), 187–211. https://doi.org/10.1016/S0169-7722(01)00158-9

Oldenburg, C. M. . (2001). *Landfill Bioreactor Model for TOUGH2*. *November*, 0–60.

Oldenburg, C. M., Borglin, S. E., & Hazen, T. C. (2002). *Multiphase modeling of flow, transport, and biodegradation in a mesoscale landfill bioreactor*. Lawrence Berkeley National Lab.(LBNL), Berkeley, CA (United States).

Pareek, S., Matsui, S., Kim, S. K., & Shimizu, Y. (1999). Mathematical modeling and simulation of methane gas production in simulated landfill column reactors under sulfidogenic and methanogenic environments. *Water Science and Technology*, *39*(7), 235–242.

Powell, J., Jain, P., Kim, H., Townsend, T., & Reinhart, D. (2006). Changes in landfill gas quality as a result of controlled air injection. *Environmental Science and Technology*, *40*(3), 1029–1034. https://doi.org/10.1021/es051114j

Pruess, K. (2004). The TOUGH codes—A family of simulation tools for multiphase flow and transport processes in permeable media. *Vadose Zone Journal*, *3*(3), 738–746.

Pruess, K., Oldenburg, C. M., & Moridis, G. J. (1999). *TOUGH2 user's guide version 2*. Lawrence Berkeley National Lab.(LBNL), Berkeley, CA (United States).

Read, A. D., Hudgins, M., Harper, S., Phillips, P., & Morris, J. (2001). The successful demonstration of aerobic landfilling. The potential for a more sustainable solid waste management approach? *Resources, Conservation and Recycling*, *32*(2), 115–146. https://doi.org/10.1016/S0921-3449(01)00053-2

Ritzkowski, M., & Stegmann, R. (2012). Landfill aeration worldwide: Concepts, indications and findings. *Waste Management*, *32*(7), 1411–1419. https://doi.org/10.1016/j.wasman.2012.02.020

Rollins, K. M., Clayton, R. J., Mikesell, R. C., & Blaise, B. C. (2005). Drilled shaft side friction in gravelly soils. *Journal of Geotechnical and Geoenvironmental Engineering*, *131*(8), 987–1003.

Rowe, R. K., & Islam, M. Z. (2009). Impact of landfill liner time-temperature history on the service life of HDPE geomembranes. *Waste Management*, *29*(10), 2689–2699. https://doi.org/10.1016/j.wasman.2009.05.010

Sanchez, R., Hashemi, M., Tsotsis, T. T., & Sahimi, M. (2006). Computer simulation of gas generation and transport in landfills II: Dynamic conditions. *Chemical Engineering Science*, *61*(14), 4750–4761. https://doi.org/10.1016/j.ces.2006.03.014

Staub, M., Galietti, B., Oxarango, L., Khire, M. V, & Gourc, J.-P. (2009). Porosity and Hydraulic Conductivity of MSW Using Laboratory-Scale Tests. *The International Workshop "Hydro-Physico-Mechanics of Landfills," March 2009*, 1–9.

Stoltz, G., Gourc, J. P., & Oxarango, L. (2010). Liquid and gas permeabilities of unsaturated municipal solid waste under compression. *Journal of Contaminant Hydrology*, *118*(1–2), 27–42. https://doi.org/10.1016/j.jconhyd.2010.07.008

Stoltz, G., Tinet, A.-J., Staub, M. J., Oxarango, L., & Gourc, J.-P. (2012). Moisture Retention Properties of Municipal Solid Waste in Relation to Compression. *Journal of Geotechnical and Geoenvironmental Engineering*, *138*(4), 535–543.

https://doi.org/10.1061/(asce)gt.1943-5606.0000616

Themelis, N. J., & Kim, Y. H. (2002). Material and energy balances in a large-scale aerobic bioconversion cell. *Waste Management and Research*, *20*(3), 234–242. https://doi.org/10.1177/0734242X0202000304

Townsend, T. G., Powell, J., Jain, P., Xu, Q., Tolaymat, T., & Reinhart, D. (2015a). *Sustainable practices for landfill design and operation*. Springer.

Townsend, T. G., Powell, J., Jain, P., Xu, Q., Tolaymat, T., & Reinhart, D. (2015b). *Sustainable Practices for Landfill Design and Operation*. Springer New York. https://doi.org/10.1007/978-1-4939-2662-6

Vigneault, H., Lefebvre, R., & Nastev, M. (2004). Numerical Simulation of the Radius of Influence for Landfill Gas Wells. *Vadose Zone Journal*, *3*(3), 909–916. https://doi.org/10.2136/vzj2004.0909

Xu, L., Lin, X., Amen, J., Welding, K., & McDermitt, D. (2014). Impact of changes in barometric pressure on landfill methane emission. *Global Biogeochemical Cycles*, *28*(7), 679–695. https://doi.org/10.1002/2013GB004571

Xu, X. B., Powrie, W., Zhang, W. J., Holmes, D. S., Xu, H., & Beaven, R. (2020). Experimental study of the intrinsic permeability of municipal solid waste. *Waste Management*, *102*, 304–311. https://doi.org/10.1016/j.wasman.2019.10.039

Yazdani, R; Kieffer, J; Sananikone, K; Augenstein, D. (2006). *"Full scale bioreactor landfill for carbon sequestration and greenhouse emission control." Final Technical Progress Report, Yolo County, Woodland, CA, USA.*

Yazdani, R., Mostafid, M. E., Han, B., Imhoff, P. T., Chiu, P., Augenstein, D., Kayhanian, M., & Tchobanoglous, G. (2010). Quantifying factors limiting aerobic degradation during aerobic bioreactor landfilling. *Environmental Science and Technology*, *44*(16), 6215–6220. https://doi.org/10.1021/es1022398

Yeşiller, N., Hanson, J. L., & Liu, W.-L. (2005). Heat Generation in Municipal Solid Waste Landfills. *Journal of Geotechnical and Geoenvironmental Engineering*, *131*(11), 1330–1344. https://doi.org/10.1061/(asce)1090-0241(2005)131:11(1330)

Yeşiller, N., Hanson, J. L., & Yee, E. H. (2015). Waste heat generation: A comprehensive review. *Waste Management*, *42*(August), 166–179. https://doi.org/10.1016/j.wasman.2015.04.004

Yortsos, Y. C. (1995). A theoretical analysis of vertical flow equilibrium. *Transport in Porous Media*, *18*(2), 107–129. https://doi.org/10.1007/BF01064674

Young, A. (1990). Volumetric changes in landfill gas flux in response to variations in atmospheric pressure. *Waste Management and Research*, *8*(5), 379–385. https://doi.org/10.1016/0734-242X(90)90077-Z

Young, A. (1992). *The effects of fluctuations in a t m o s p h e r i c pressure o n l a n d f i l l gas m i g r a t i o n and c o m p o s i t i o n*. 601–616.

Zambra, C. E., Moraga, N. O., & Escudey, M. (2011). Heat and mass transfer in unsaturated porous media: Moisture effects in compost piles self-heating. *International Journal of Heat and Mass Transfer*, *54*(13–14), 2801–2810. https://doi.org/10.1016/j.ijheatmasstransfer.2011.01.031

Zekkos, D., Bray, J. D., Kavazanjian, E., Matasovic, N., Rathje, E. M., Riemer, M. F., & Stokoe, K. H. (2006). Unit Weight of Municipal Solid Waste. *Journal of Geotechnical and Geoenvironmental Engineering*, *132*(10), 1250–1261. https://doi.org/10.1061/(asce)1090-0241(2006)132:10(1250)

Zinder, S. H. (1993). Physiological ecology of methanogens. In *Methanogenesis* (pp. 128–206). Springer.

Table 1. Summary of material properties for MSW and clay layers

Material Properties	Unit	Shallow MSW	Intermediate MSW	Deep MSW	Clay
Bulk Density, ρ	kg/m^3	750	920	1110	1200
Porosity, n	-	0.6	0.5	0.4	0.7

Permeability, k_x[1]	m^2	3.8×10^{-11}	3.8×10^{-12}	3.8×10^{-13}	1×10^{-15}
Permeability, k_z[2]	m^2	3.8×10^{-12}	3.8×10^{-13}	3.8×10^{-14}	1×10^{-16}
Thermal conductivity, K_T	W/(m·K)	0.3	0.6	0.9	2.1
Heat capacity, C_p	J/(kg·K)	1080-3000	1080-3000	1080-3000	935.8
Grid counts	-	1528	2653	1914	370

[1] Horizontal intrinsic permeability
[2] Vertical intrinsic permeability

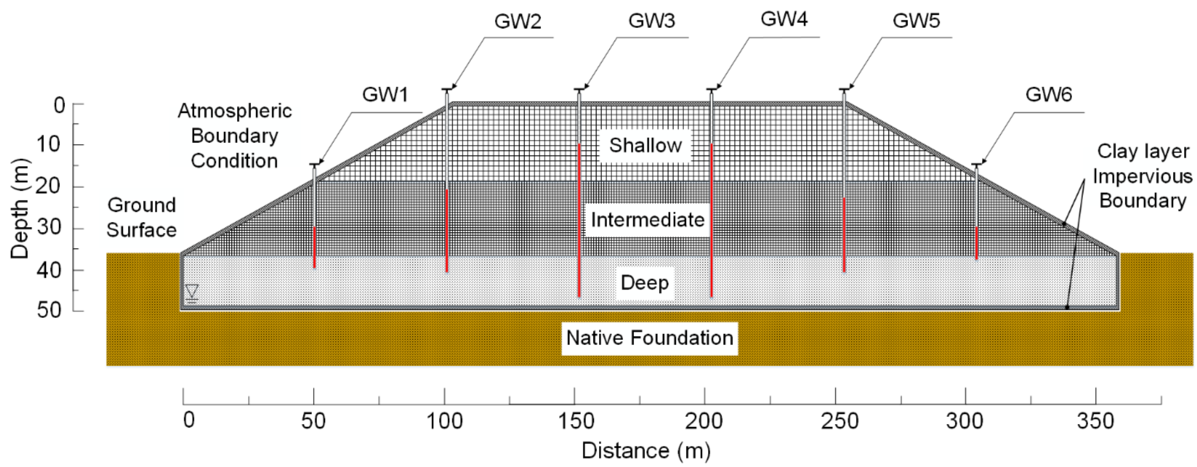

Fig. 1. Cross-section of the idealized landfill system consisting of three MSW layers and six gas extraction wells (red color indicates gas well slot length). Figure is not to scale.

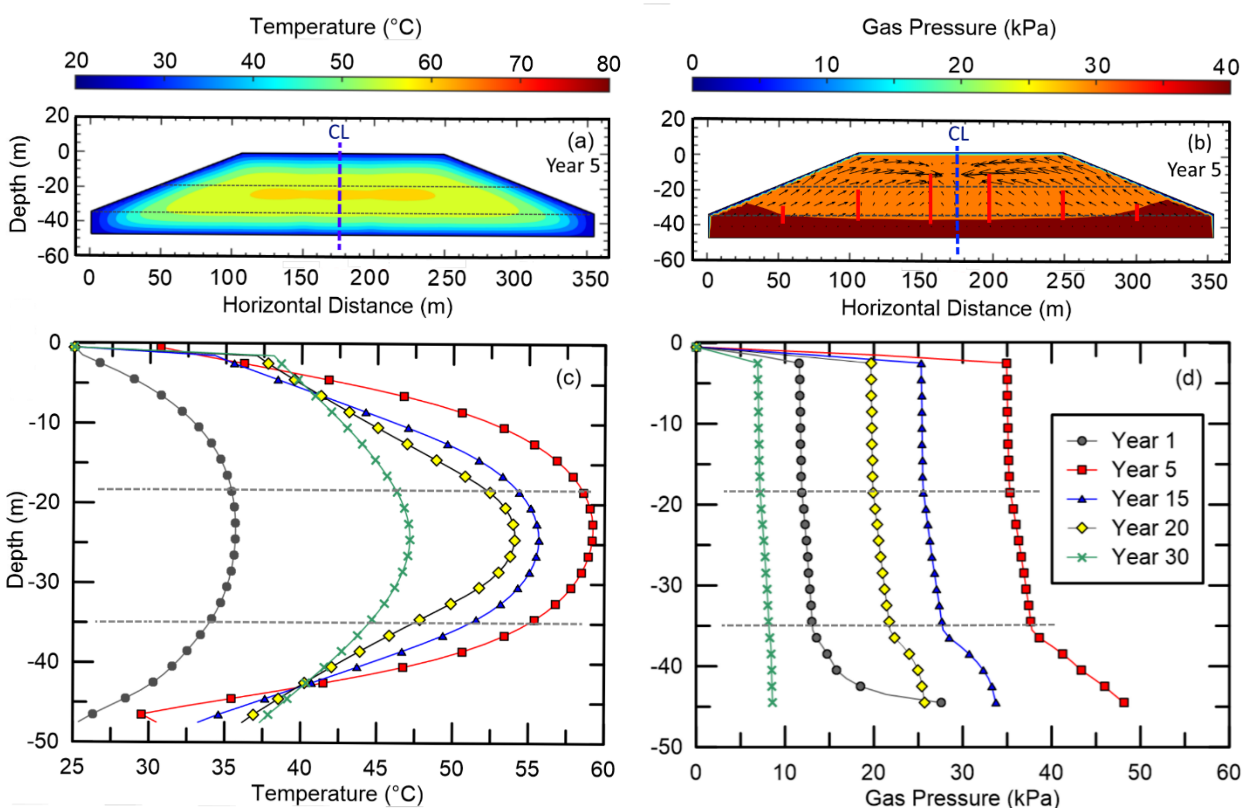

Fig. 2. Temporal changes at the center of the landfill: (a and c) Temperature, and (b and d) Gas pressure. The intersections of MSW layers are showed with dashed lines and the gas collection wells are signified by vertical red lines.

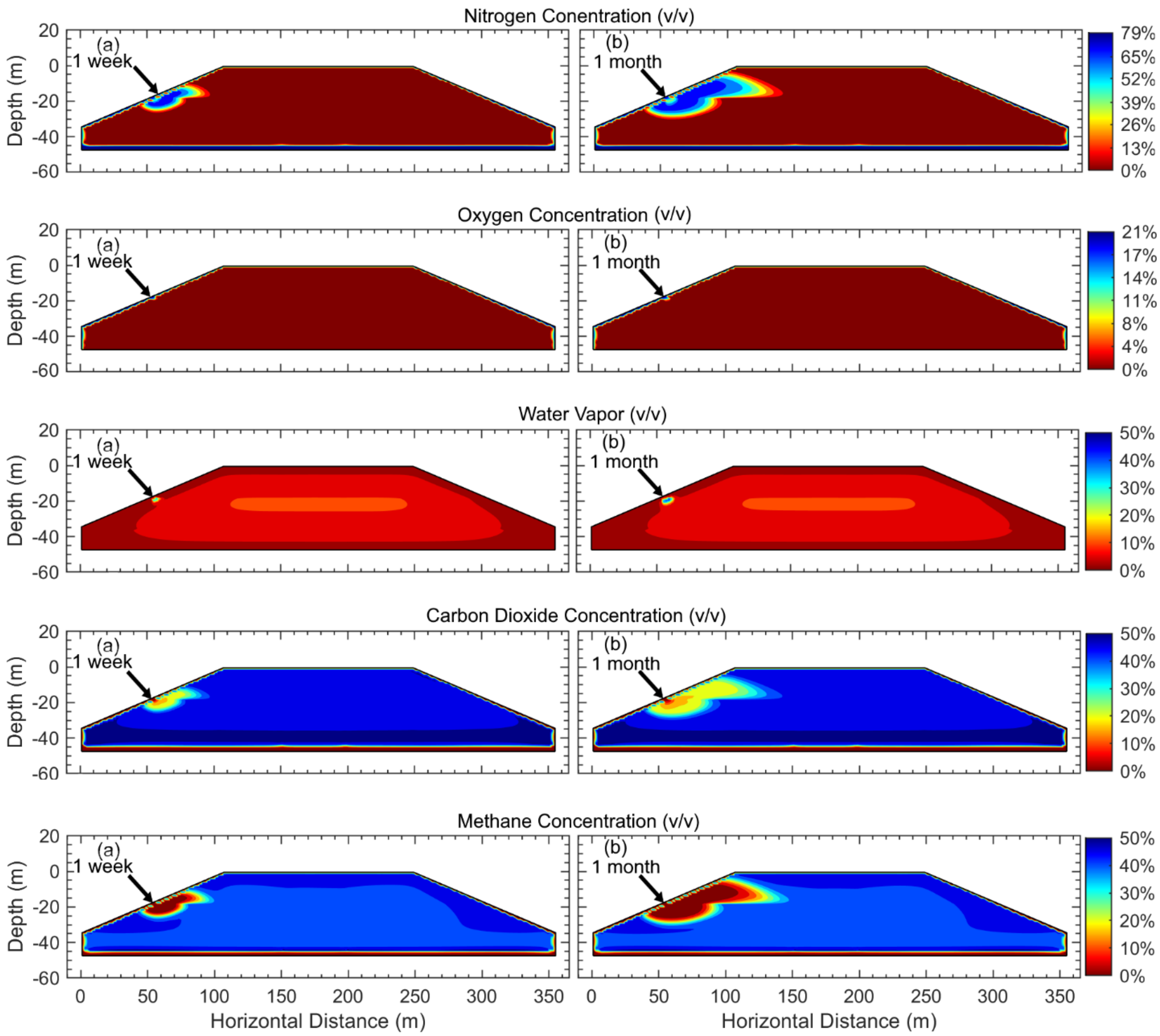

Fig. 3. Spatial distribution of gas composition after 1 week and 1 month of air intrusion. The air intrusion location is indicated by the arrow.

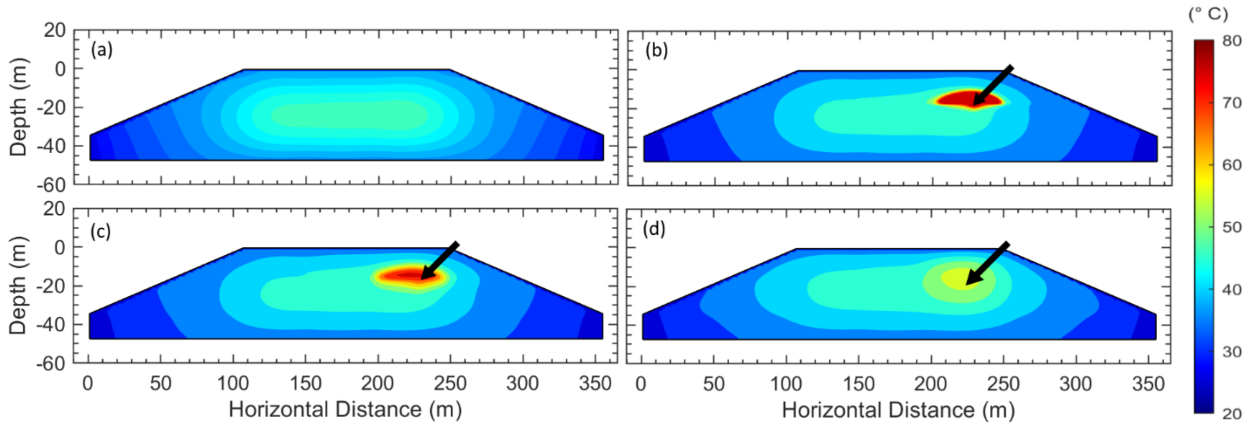

Fig. 4. Temperature development during Scenario 2: (a) Initial anaerobic conditions, (b) after 1 week of air intrusion, (c) 1 month after repairing the leak, and (d) 1 year after the air line break. The air line break is indicated by the arrow.

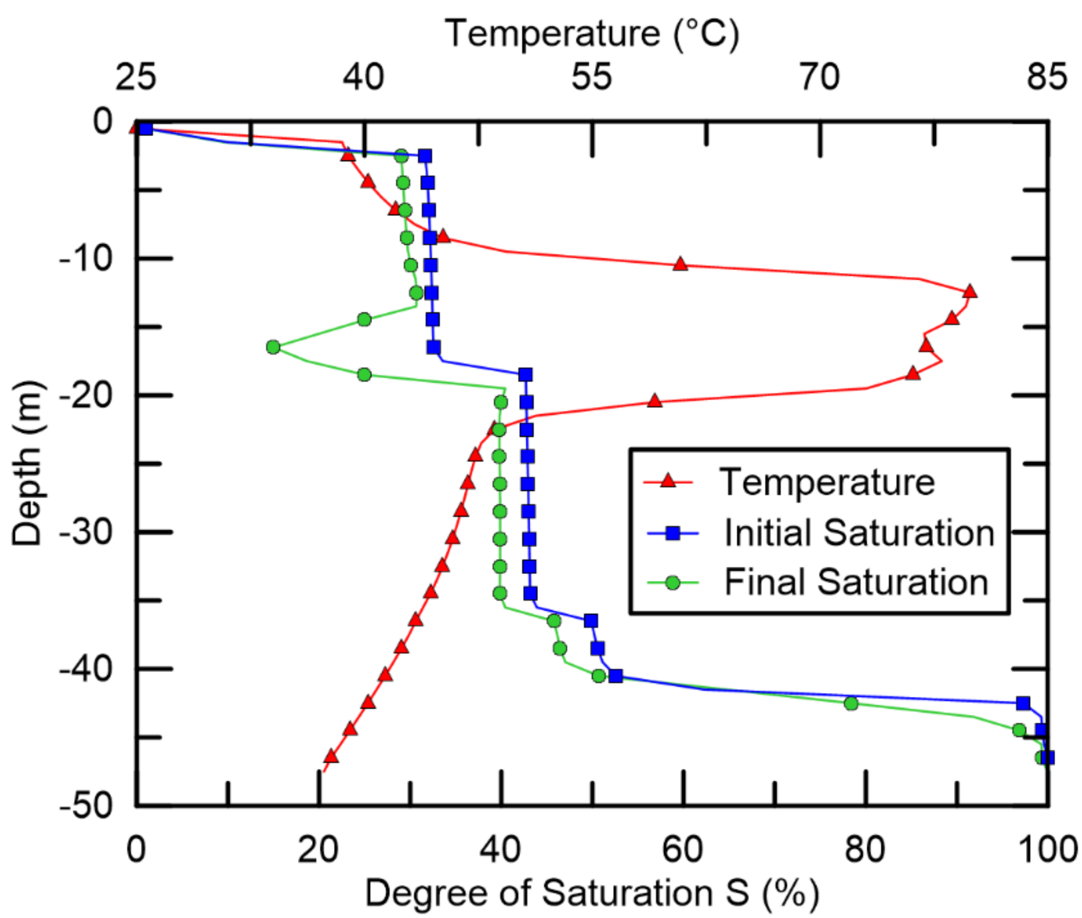

Fig. 5. Temperature and degree of saturation profiles after one week of air leak along the depth at the location of air line break.

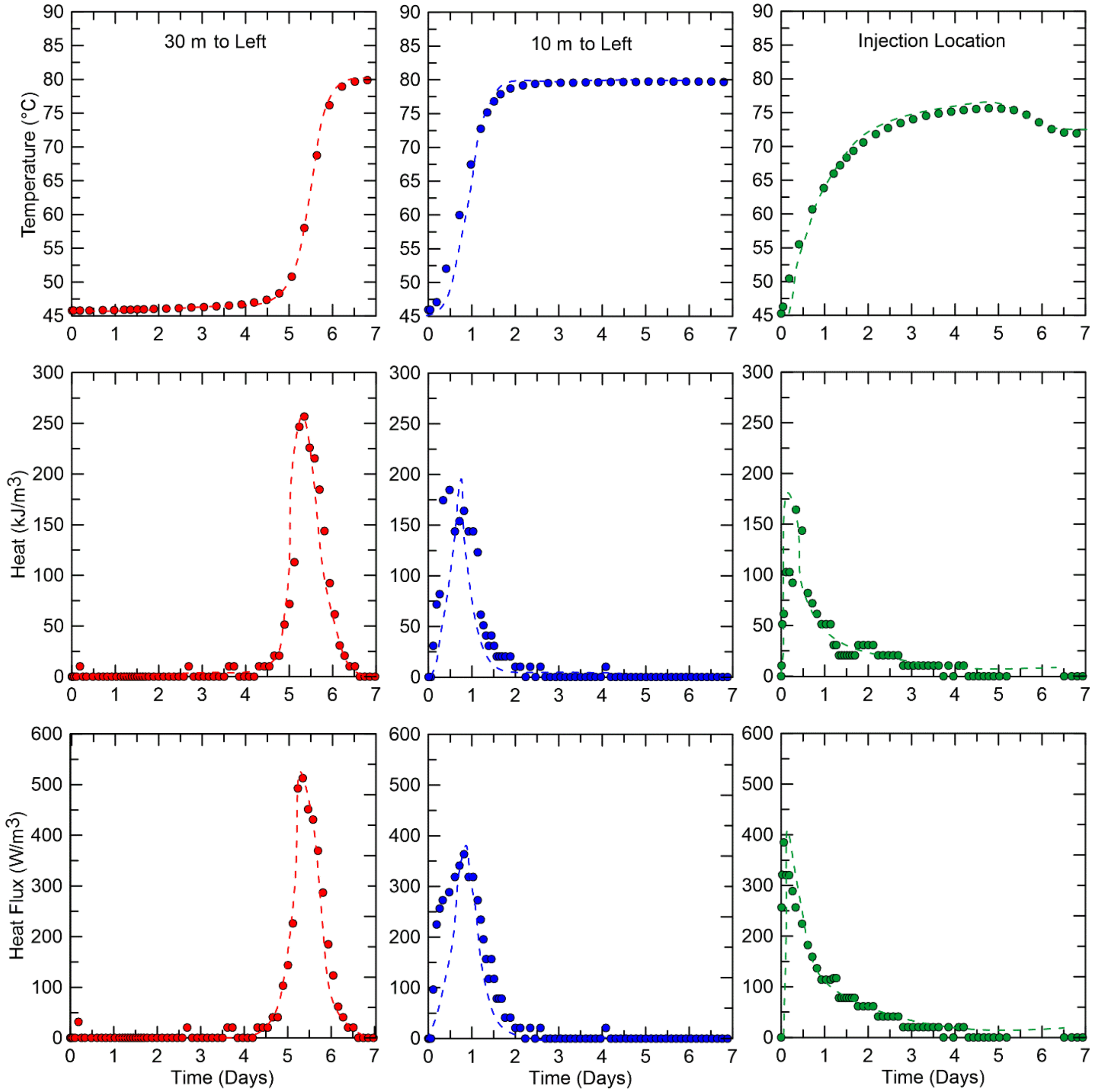

1061
1062 **Fig. 6.** Horizontal variation of temperature, heat of enthalpy, and heat flux during 1 week of air
1063 line break.
1064

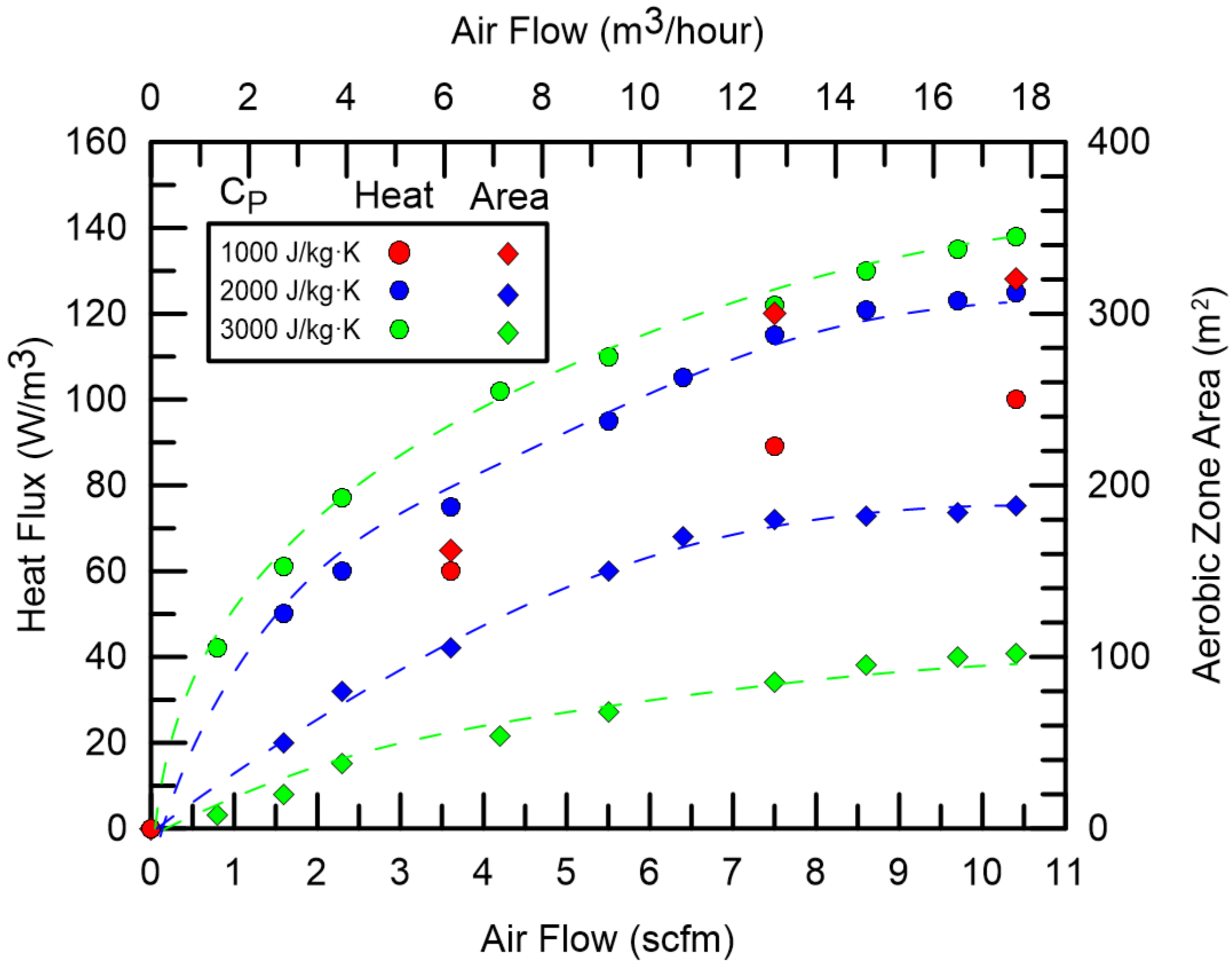

Fig. 7. Sensitivity of heat generation and aerobic zone area as a function of heat capacity and air flow after one week of air injection into MSW.

SUPPLEMENTARY MATERIAL

NUMERICAL INVESTIGATION OF AIR INTRUSION AND AEROBIC REACTIONS IN MUNICIPAL SOLID WASTE LANDFILLS

Alborz Fathinezhad
Dept. of Civil and Environmental Engineering
Louisiana State University
Baton Rouge, LA 70803
Email: falbor1@lsu.edu

Navid H. Jafari, Ph.D., A.M. ASCE
Assistant Professor of Civil and Environmental Engineering
Louisiana State University
Baton Rouge, LA 70803
Email: njafari@lsu.edu

Curtis M. Oldenburg, Ph.D.
Senior Scientist
Energy Geosciences Division
Lawrence Berkeley National Laboratory
Email: cmoldenburg@lbl.gov

Michael D. Caldwell
Director, Groundwater and Technical Program
Waste Management, Inc.
Houston, TX
Email: mcaldwell@wm.com

Open Access version of the Supplementary Material for the published paper:

Fathinezhad, A., Jafari, N.H., Oldenburg, C.M. and Caldwell, M.D., 2022. Numerical investigation of air intrusion and aerobic reactions in municipal solid waste landfills. *Waste Management*, *147*, pp.60-72.
https://doi.org/10.1016/j.wasman.2022.05.009

October 3, 2022

Fig. S1 shows the degree of saturation (S) as a function of matric suction (ψ) for each material layer, and Table S1 lists the TOUGH2 input parameters for van Genuchten (1980) function.

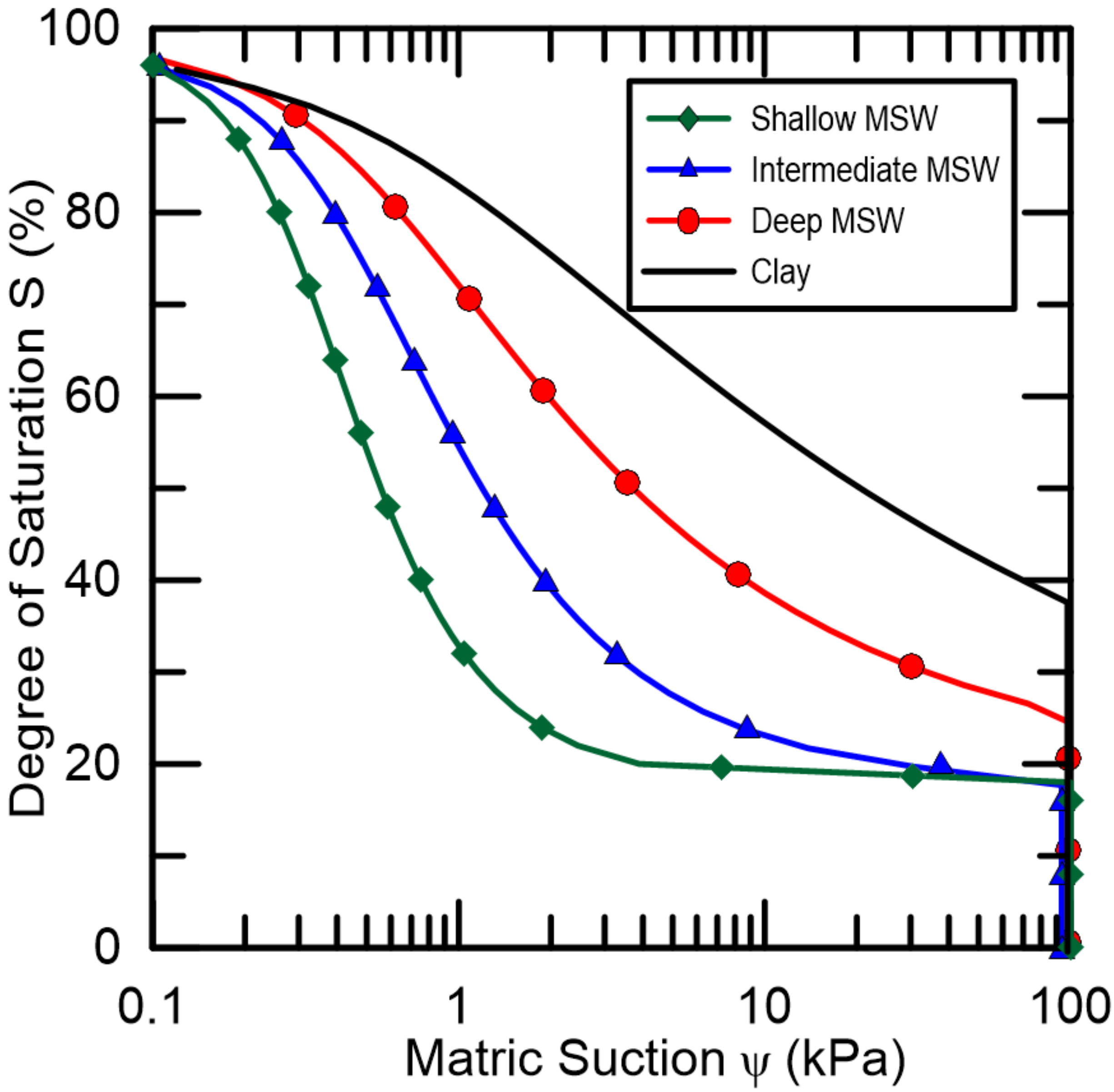

Fig. S8. ***SWRC for the three MSW and clay layers in the model landfill system.***

First, gravity capillary equilibrium is simulated in a 1-D column spanning the height of the landfill from bottom liner to surface cover, with 48 grid blocks composed of one MSW layer and a water table that is assigned at a depth of 47 m. The water-table single grid block in this step is assigned a volume of 1×10^{50} m^3, high permeability, and zero capillary pressure to ensure this grid block permanently remains saturated and avoids any changes in the hydrostatic leachate level. The other 47 grid blocks are assigned a volume of 2 m^3 and regular capillary pressure based on the values in Table S1 and results shown in Fig. S1. The simulation time for this step must be extremely large, more than 100 years, such that the capillary fringe level reaches to the top layers of the landfill and a steady state is achieved. The next step consists of changing the large-volume of the water-table grid block back to 2 m^3 and assigning no-flux boundary conditions (second-type boundary condition) of the clay cover layer by manually changing the properties and saturation level of the top-layer and bottom-layer grid blocks to match those from the gravity capillary steady-state and again running the simulation for 100 years. Finally, the atmospheric boundary condition was assigned to the top grid block by prescribing constant pressure and temperature to 101 kPa and 25 °C, respectively as the first-type boundary condition.

The next step accounts for the landfill side slopes and the slight change in atmospheric gas density, which is achieved by replicating the 1-D column across the 2-D rectangular model. The grid blocks not associated with the landfill (i.e., above the sloping cover system) are subsequently deleted. The last step is to assign the specified MSW properties in Table 1 and supplementary Table 2 to relevant grid blocks and then rerunning the system to gravity-capillary equilibrium. The result of this series of steps is the static gravity-capillary equilibrium shown in Fig. S2, where the blue dashed line is showing the degree of saturation along the depth. The degree of saturation is nearly zero at the top cover and 31% in the shallow layer, 45% in the intermediate layer, 50% to 99% in the deep layer, and 100% at the top of the bottom clay layer where the water table (leachate level) is located. The red line in Fig. S2 indicates the corresponding capillary pressure with depth based on the SWRC shown in Fig. S1.

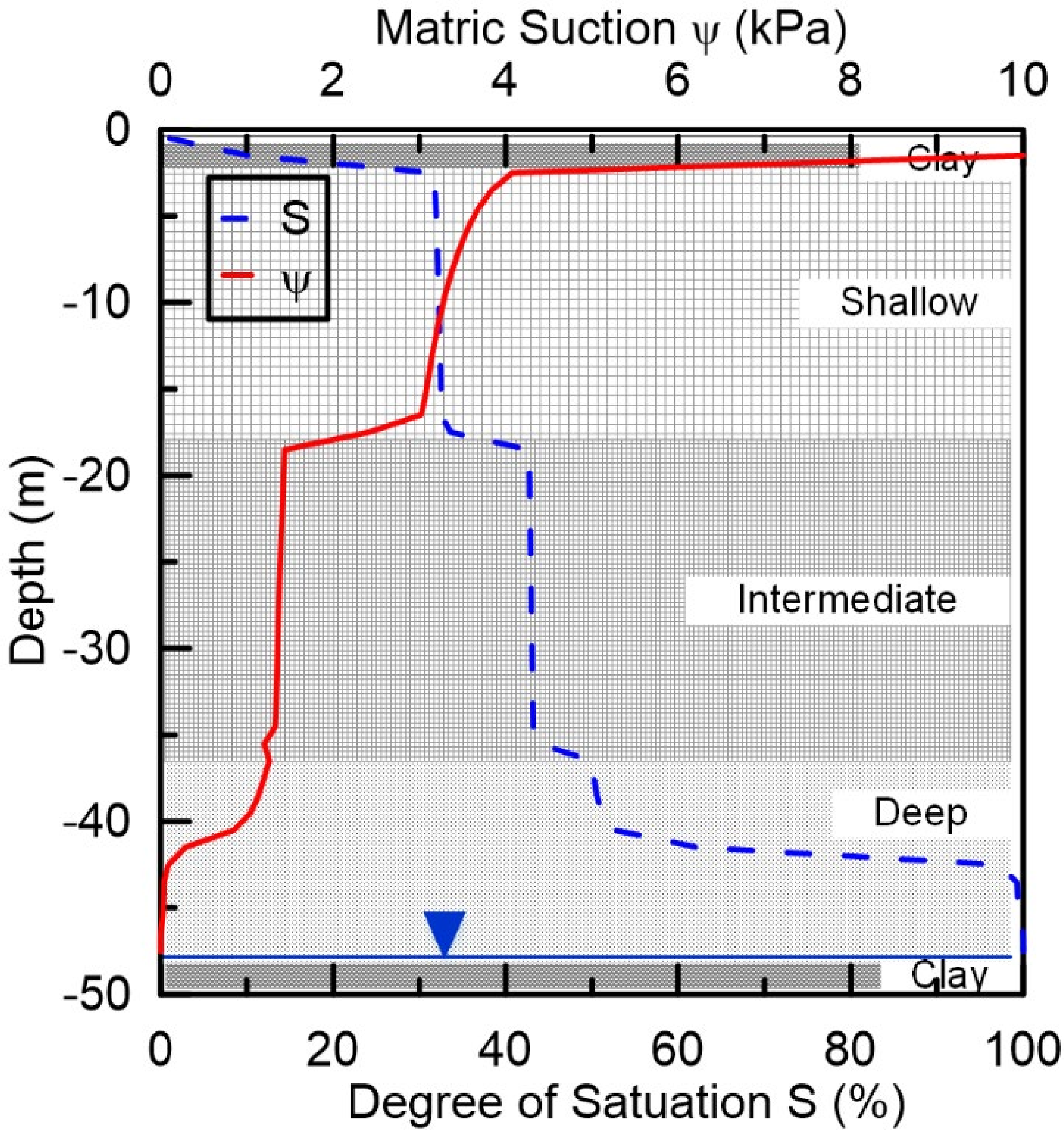

Fig. S9. ***Simulated static gravity-capillary equilibrium showing the unsaturated zone matric suction and degree of saturation that are used as the initial condition for subsequent biodegradation and air-intrusion processes.***

In the T2LBM model system, the gas pressure builds up quickly (20 to 30 kPa) between years 5 to 20, which correspond to the period with highest gas generation rate as shown in supplementary Fig. S3. Steady-state gas pressures are reached after 30 years, where the pressure is slightly higher than atmospheric pressure. The pressure distribution in supplementary Fig. S4 shows a constant profile with depth, which may be attributed to the gas extraction wells redistributing gas from high to low pressure. There are limited gas pressure measurements in landfills to validate the simulated gas pressures shown in supplementary Fig. S4. Anecdotal evidence of landfill gas operations suggests that biogas can accumulate under the interim cover system, leading to bulges in geomembrane liners.

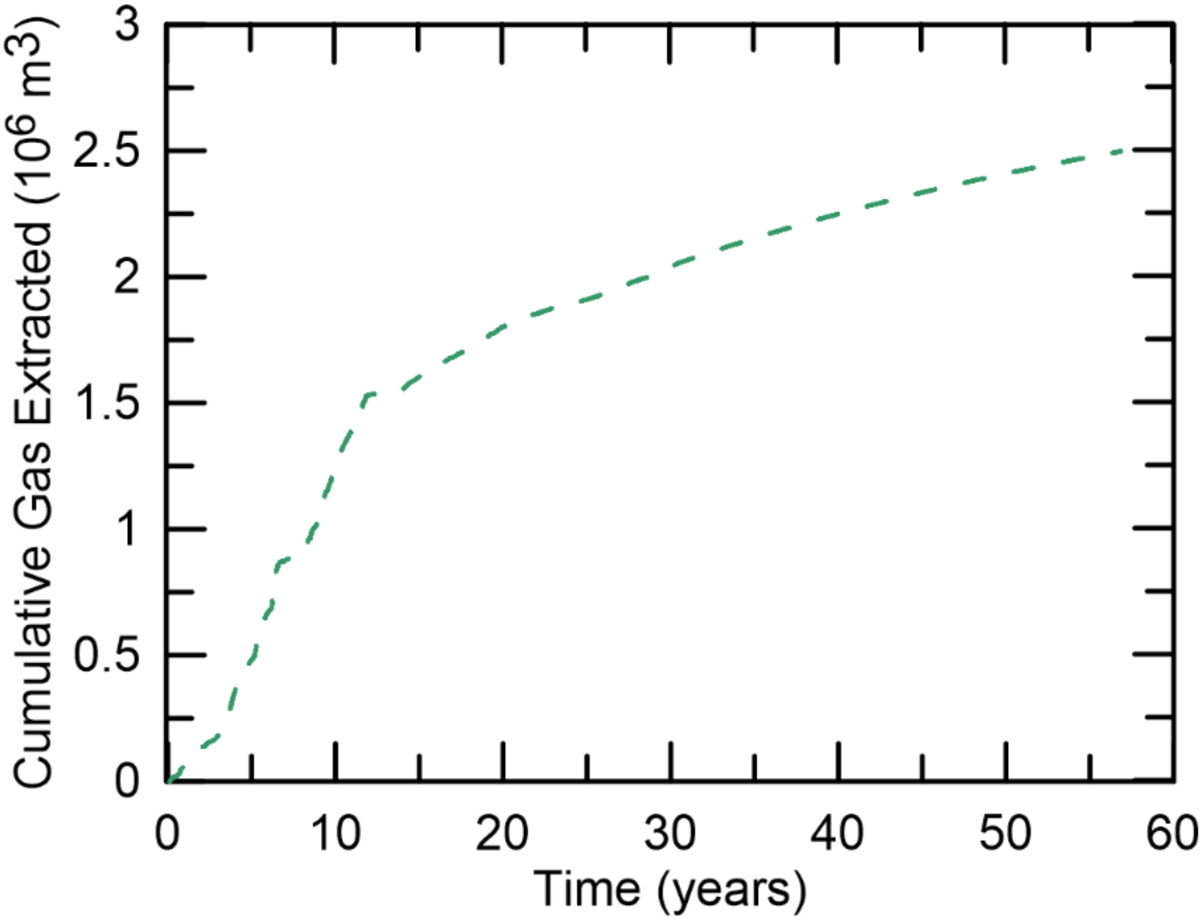

Fig. S10. ***Cumulative gas extracted due to anaerobic MSW biodegradation.***

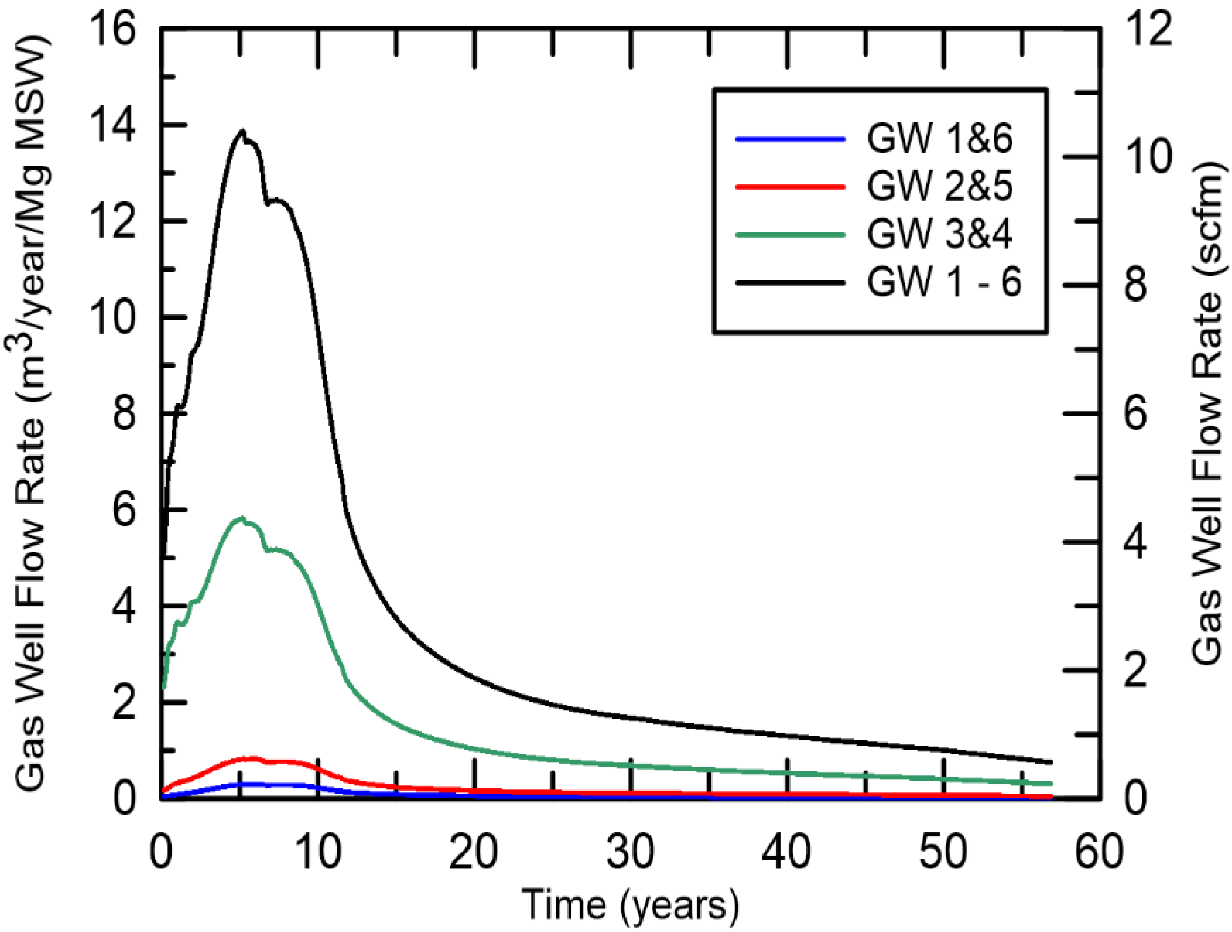

Figure S11. ***Gas well collection performance during the anaerobic biodegradation period.***

Fig. S5 shows the temperature contours inside the landfill at years 1, 5, 15, and 30, which are parabolic with the maximum temperature in the middle depth.

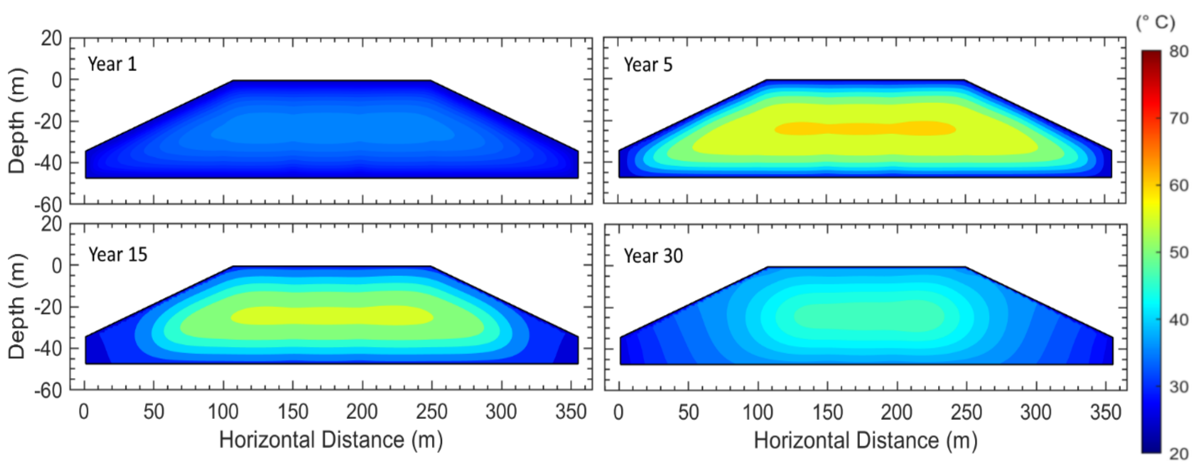

Fig. S12. ***Temperature evolution during anaerobic biodegradation.***

The simulated anaerobic temperature profile was calibrated based on the real landfill temperature profile. In Fig. S6, MSW temperatures in the month of February approached 76°C (170 °F) in the middle of the landfill. The impetus for using this temperature data was to replicate the temperature profile with depth. The objective was not to match the actual temperatures.

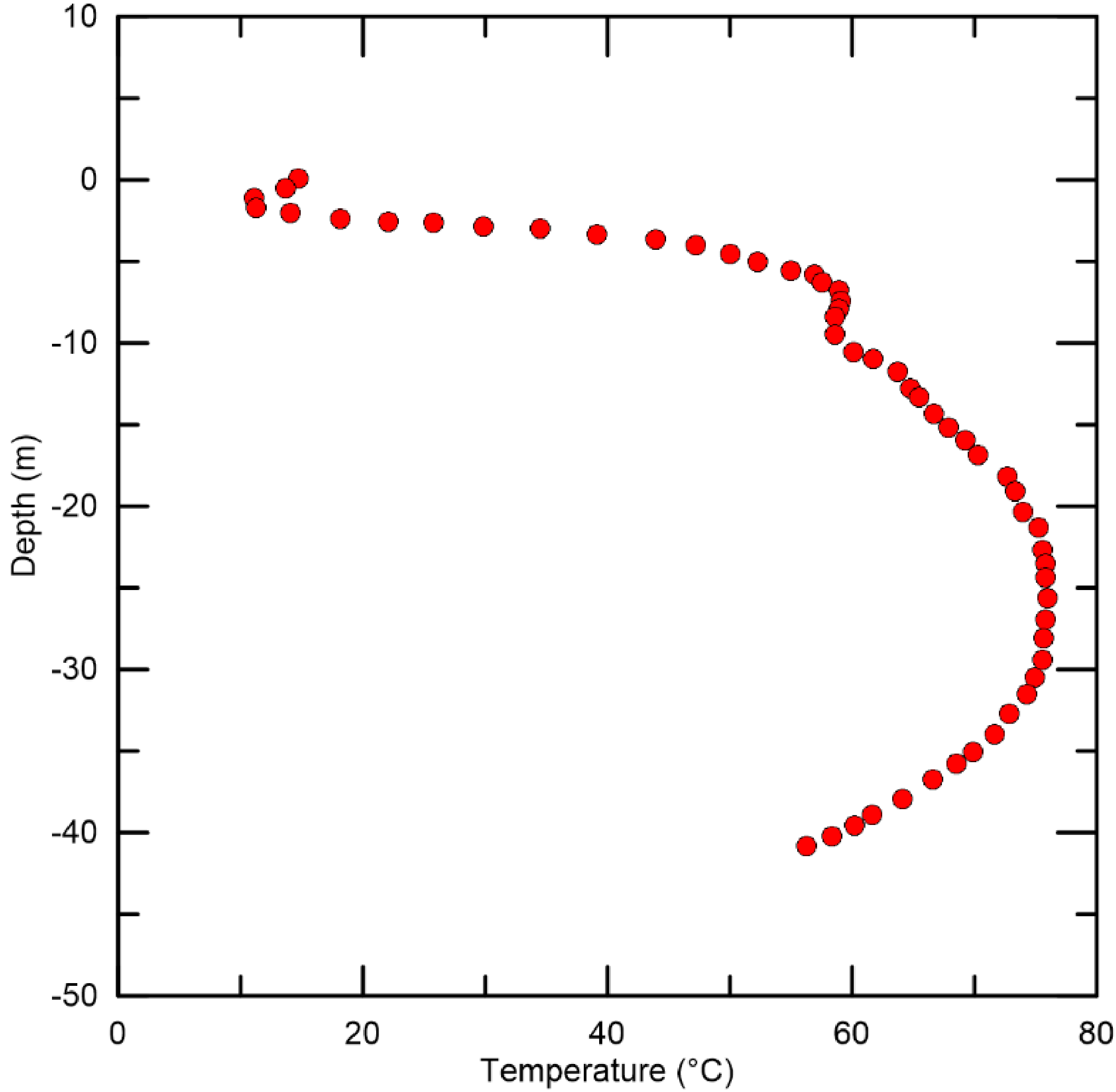

Fig. S13. ***Real Landfill Temperature Profile***

Fig. S7 shows the gas pressure contours inside the landfill at years 1, 5, 15, and 30, and the arrows show the direction of landfill biogas flowing towards the gas collection wells. Large arrows at the shallow layer represent the higher gas flow rates compared to the small arrows in the deep layer.

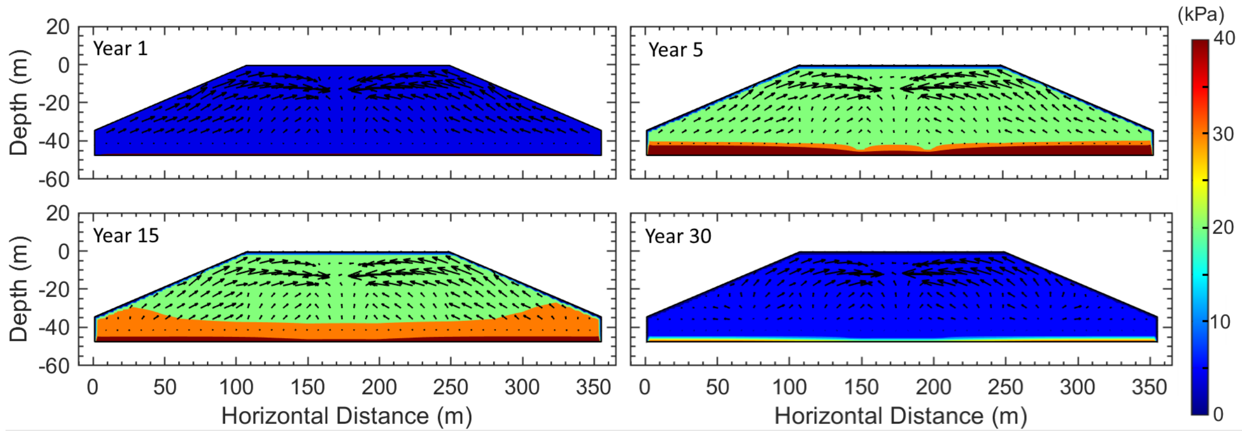

Fig. S14. ***Pressure evolution during anaerobic biodegradation***

Simulation results in Fig. S8(a) show the landfill operating under a steady anaerobic condition with average temperature profiles reported in Fig. 2. Air intrusion occurs because of a pressure differential of 5 kPa combined with a single grid block of the clay cover simulated as a high-permeability material to reflect a crack. This leads air flowing into MSW with rate of 0.34 m^3/hour (0.2 scfm).

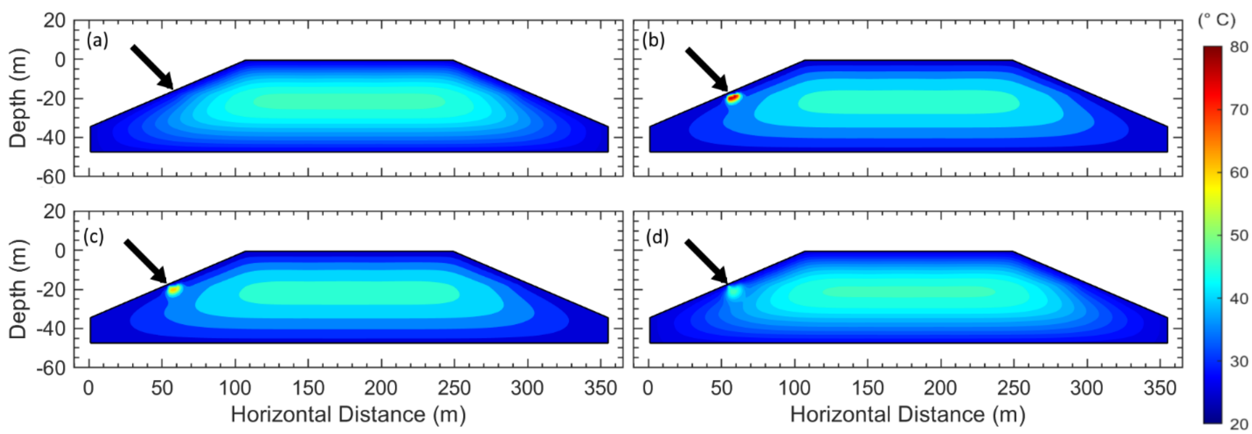

Fig. S8. ***Temperature development during an air intrusion from crack in surface clay cover: (a) Initial normal landfill temperature, (b) after one month of air intrusion, (c) one month after repairing the opening, and (d) one year after the repair of the opening. The air intrusion location is shown by the arrow.***

In Fig. S9(a), the time-history of biogas production is compared before and after air intrusion.

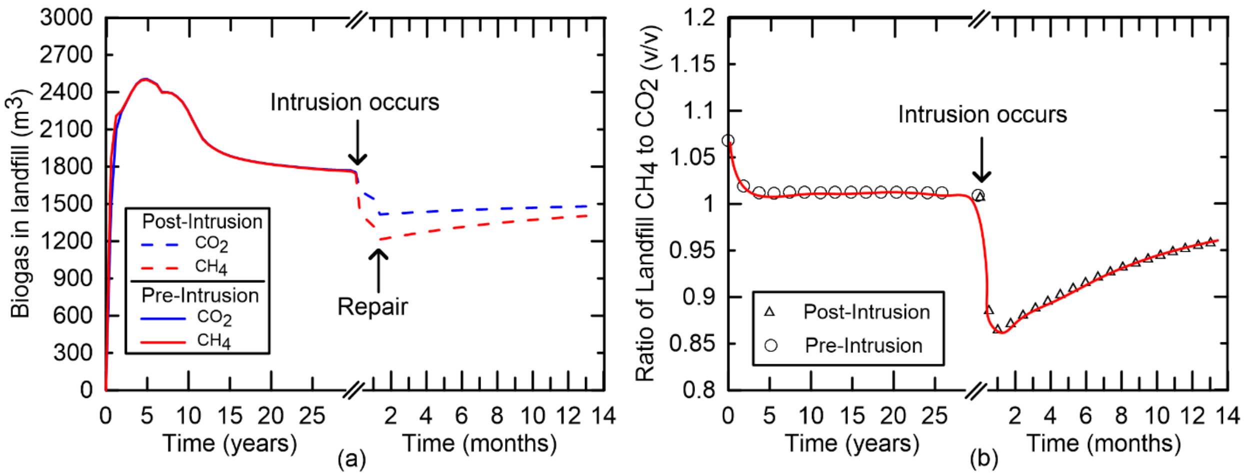

Fig. S9. ***Pre- and post-intrusion landfill biogas composition.***

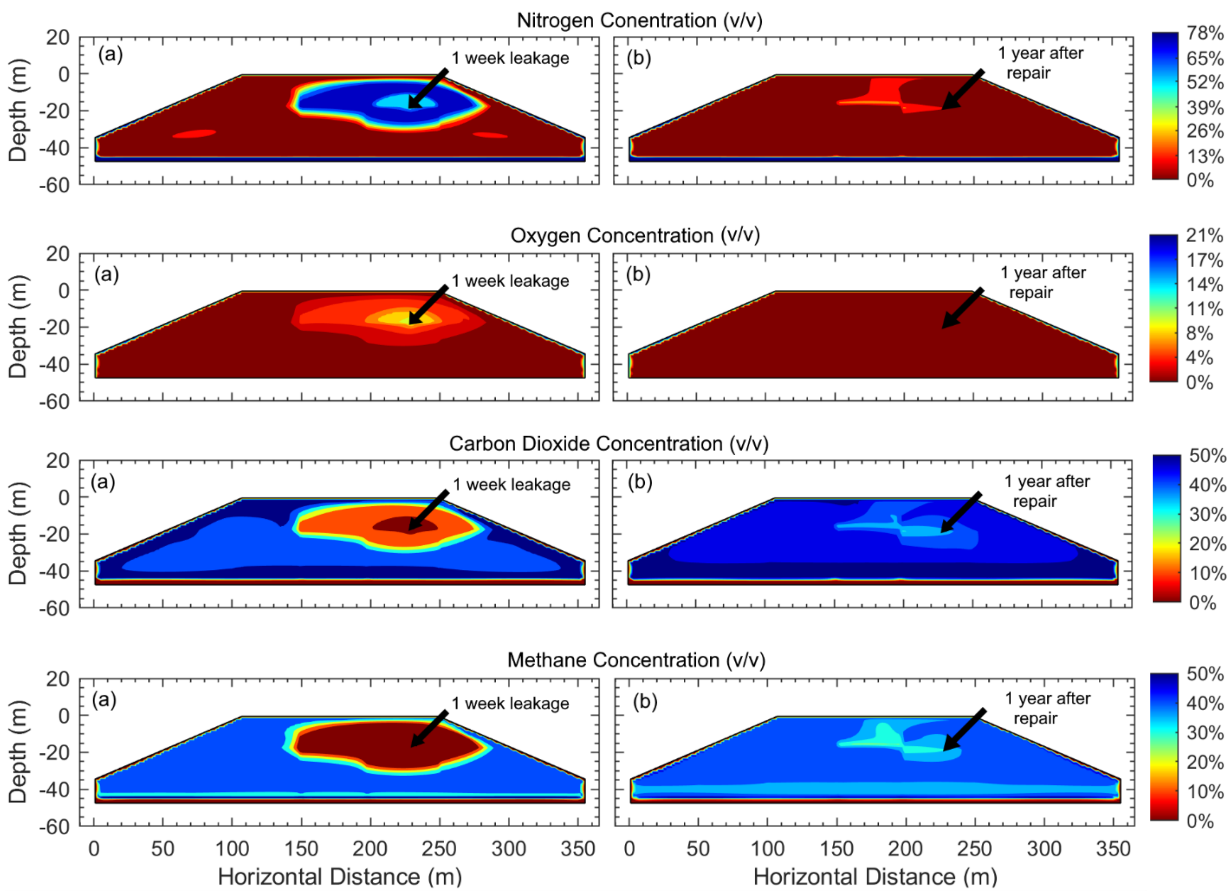

Fig. S10. ***Spatial distribution of landfill gas composition during 1 week of air line break and 1 year after the repair. The arrow points to the location of the air line break.***

To calculate the average heat flux generated by each individual grid block, the area under dashed line (in Fig. 6) was divided by the time of occurrence. For example, for the 30 m grid block, the area under dashed line was ~ 360 W·day/m^3 and then divided by 2 days of heat generation (day 4.5 to day 6.5), we estimated ~180 W/m^3 as the average heat flux. The same approached was used to calculate the average heat flux of each grid block inside of the aerobic zone. Then, we summed and averaged within all the grid blocks. Results are shown int the figure below for four (4) air flow rates.

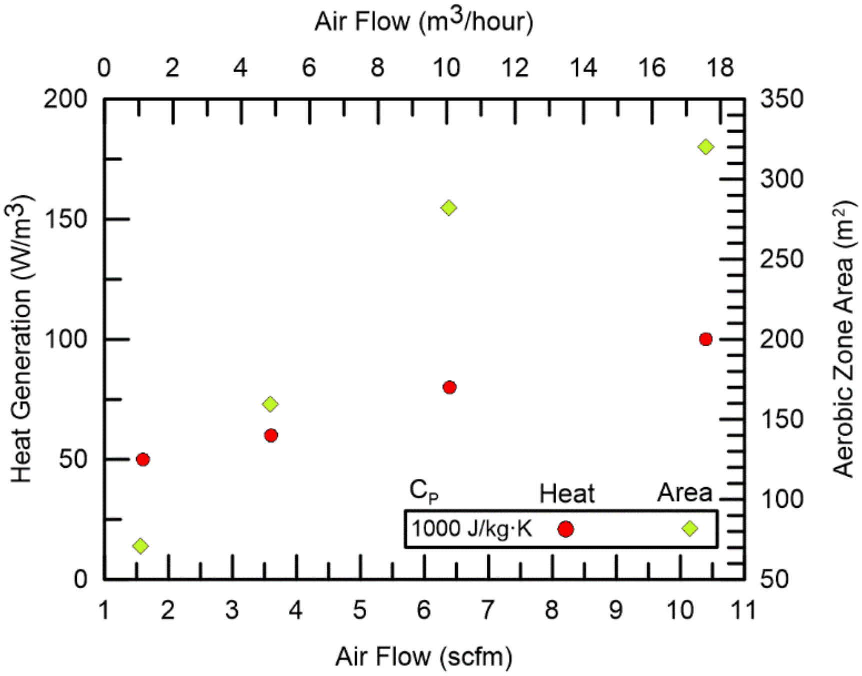

Fig. S11. Comparison of heat generation and impacted area of aerobic biodegradation in MSWs with specific heat capacity of 1000 J/(kg·K) and 2000 J/(kg·K).

Table S2. ***Summary of van Genuchten parameters for clay and MSW layers.***

van Genuchten Parameter	Shallow MSW		Intermediate MSW		Deep MSW		Clay layer	
	R.P.[1]	**C.P.**[2]	**R.P.**	**C.P.**	**R.P.**	**C.P.**	**R.P.**	**C.P.**

$\lambda^{(3)}$	0.61	0.6	0.41	0.45	0.31	0.3	0.21	0.2
S_{lr}	0.31	0.35	0.41	0.3	0.34	0.3	0.11	0.1
S_{ls}	1	1	1	1	1	1	1	1
S_{gr}	5×10^{-3}	---	5×10^{-3}	---	5×10^{-3}	---	0.02	---
$1/P_0$[4]	---	3×10^{-3}	---	3×10^{-3}	---	3×10^{-3}	---	8×10^{-4}
P_{max} (kPa)[5]	---	100	---	100	---	100	---	100

[1] Relative Permeability functions parameters.
[2] Capillary Pressure functions parameters.
[3] Parameter λ is m in van Genuchten's (1980) notation in TOUGH2, where $m = 1 - 1/n$ (m and n are the empirical shape-defining and dimensionless parameters in the van Genuchten equation).
[4] Equal to $\alpha/(\rho_w \times g)$
[5] P_{max} is implemented as an upper boundary based on available field observations that suggest landfill matric suction values are low (Breitmeyer 2011).

The parameters used in Eq. 8. and fitted values are listed in Table S2.

Table S3. ***Summary of gas extraction well input properties.***

Well ID	***PI* (m^3) in MSW layer**			**Slot length (m) in MSW layer**			**P_{wb}**
	Deep	**Intermediate**	**Shallow**	**Deep**	**Intermediate**	**Shallow**	**(kPa)**
GW1	3.86×10^{-12}	9.05×10^{-11}	---	3	7	---	95
GW2	6.46×10^{-12}	2.32×10^{-10}	1.29×10^{-11}	5	18	1	95
GW3	1.16×10^{-11}	2.32×10^{-10}	1.16×10^{-09}	9	18	9	95
GW4	1.16×10^{-11}	2.32×10^{-10}	1.16×10^{-09}	9	18	9	95
GW5	6.46×10^{-12}	1.81×10^{-10}	1.29×10^{-12}	5	18	1	95
GW6	1.03×10^{-10}	---	---	8	---	---	95

The kinetic parameters used for aerobic and anerobic biological reactions are listed in Table S3.

Table S4. ***Biological parameters used in T2LBM model***

Parameter	**Unit**	**Anaerobic**	**Aerobic**
Yield coefficient, Y	kg/kg of MBSP	0.2	0.2
Maximum growth rate, μ_{max}	Day^{-1}	0.16	20
Inhibiting temperature	ºC	65	80
Saturation constant of microbes	kg/kg of aqueous phase	8×10^{-3}	8×10^{-3}
Microbial death (decay) rate, δ	Day^{-1}	0.06	0.6
Initial microbes fraction	kg/kg of aqueous phase	1×10^{-4}	1×10^{-4}
Enthalpy of bioreaction	MJ/kg of MBSP	1.0	15
Critical oxygen concentration	kg/kg of aqueous phase	---	1.8×10^{-7}